The Tropopause and the Thermal Stratification in the Extratropics of a Dry Atmosphere

Tapio Schneider

California Institute of Technology, Pasadena, California

ABSTRACT

A dynamical constraint on the extratropical tropopause height and thermal stratification is derived by considerations of entropy fluxes, or isentropic mass fluxes, and their different magnitudes in the troposphere and stratosphere. The dynamical constraint is based on a relation between isentropic mass fluxes and eddy fluxes of potential vorticity and surface potential temperature and on diffusive eddy flux closures. It takes baroclinic eddy fluxes as central for determining the extratropical tropopause height and thermal stratification and relates the tropopause potential temperature approximately linearly to the surface potential temperature and its gradient.

Simulations with an idealized GCM point to the possibility of an extratropical climate in which baroclinic eddy fluxes maintain a statically stable thermal stratification and, in interaction with large-scale diabatic processes, lead to the formation of a sharp tropopause. The simulations show that the extratropical tropopause height and thermal stratification are set locally by extratropical processes and do not depend on tropical processes and that, across a wide range of atmospheric circulations, the dynamical constraint describes the relation between tropopause and surface potential temperatures well. An analysis of observational data shows that the dynamical constraint, derived for an idealized dry atmosphere, can account for interannual variations of the tropopause height and thermal stratification in the extratropics of the earth's atmosphere.

The dynamical constraint implies that if baroclinic eddies determine the tropopause height and thermal stratification, an atmosphere organizes itself into a state in which nonlinear interactions among eddies are inhibited. The inhibition of nonlinear eddy–eddy interactions offers an explanation for the historic successes of linear and weakly nonlinear models of large-scale extratropical dynamics.

1. Introduction

The troposphere is the atmospheric layer within which the circulation redistributes the bulk of the entropy (heat) that the atmosphere receives by the heating at the surface. In fluid dynamical parlance, the troposphere is the caloric boundary layer of the atmosphere, with the tropopause as the upper boundary of this layer. The height of the tropopause and the thermal stratification of the troposphere are determined by a dynamical equilibrium between radiative processes and dynamic entropy fluxes. For the Tropics, the fundamental significance of moist convection for the entropy transport and for determining the tropopause height and thermal stratification are well established. But despite decades of experimentation with general circulation models, the dynamics that determine the tropopause height and thermal stratification in the extratropics have remained obscure.

Held (1982) suggested subdividing theories of the tropopause height and thermal stratification into two parts: a radiative constraint and a dynamical constraint. The radiative constraint takes for each latitude a measure of the tropospheric thermal stratification (e.g., the temperature lapse rate) and a lower boundary condition (e.g., the temperature or potential temperature at the surface) as given and determines the tropopause height by radiative transfer considerations. The tropopause height at each latitude is determined as the minimum height at which the tropospheric temperature profile that is consistent with the measure of the thermal stratification and with the lower boundary condition matches a radiative equilibrium temperature profile that implies the same amount of upwelling longwave radiation at the tropopause as the tropospheric temperature profile. That is, to determine the tropopause height, one assumes the stratosphere to be approximately in radiative equilibrium. Thuburn and Craig (1997, 2000) have shown in a series of GCM simulations that, if one takes a representative latitude-dependent temperature lapse rate and the surface temperature as given, radiative constraints of this kind can approximately account for the tropopause height.

The dynamical constraint provides the measure of the tropospheric thermal stratification that is taken as given

Corresponding author address: Tapio Schneider, California Institute of Technology, Mail Code 100-23, 1200 E. California Blvd., Pasadena, CA 91125.
E-mail: tapio@gps.caltech.edu

in the radiative constraint. For the Tropics, the fact that moist convection maintains the temperature lapse rate close to the moist pseudoadiabatic lapse rate (Xu and Emanuel 1989) provides such a dynamical constraint. The difficulty in accounting for the extratropical tropopause height and thermal stratification has its roots in the lack of a dynamical constraint of comparable simplicity for the extratropics. If a dynamical constraint for the extratropics were available, the temperature distribution in the extratropical troposphere and the tropopause height could be computed from a radiative constraint of the kind discussed by Thuburn and Craig, provided the temperature or potential temperature at the surface is taken as given or can be inferred from energy balance considerations.

Baroclinic eddies constitute central elements in the dynamical constraints on the extratropical tropopause height and thermal stratification that have been proposed. For example, according to baroclinic adjustment hypotheses, baroclinic eddies maintain the thermal stratification of the extratropical troposphere in a state that is neutral with respect to linear baroclinic instability (see, e.g., Stone 1972, 1978; Lindzen and Farrell 1980; Lindzen 1993). A priori, however, there is no reason to expect that baroclinic eddies would maintain the extratropical atmosphere in a state that is neutral with respect to linear baroclinic instability; baroclinic instability can equilibrate nonlinearly, which can result in a dynamical equilibrium that is linearly unstable (see, e.g., Vallis 1988). As an alternative to baroclinic adjustment hypotheses, Juckes (2000) has proposed a dynamical constraint that takes the sporadic moist convection in warm sectors of surface cyclones as the determinant of the tropospheric thermal stratification. In contrast to baroclinic adjustment hypotheses, Juckes's dynamical constraint takes convective influences on the extratropical thermal stratification into account and does not presuppose the equilibration of baroclinic eddies to be weakly nonlinear (as the equilibration would have to be to result in a baroclinically neutral dynamical equilibrium). A similar proposal in which slantwise moist convection plays a central role in determining the extratropical tropopause height and thermal stratification has been made by Emanuel (1988, 2002).

In this paper, a dynamical constraint is proposed that, like baroclinic adjustment hypotheses, is based on the premise that baroclinic eddies are central for determining the extratropical tropopause height and thermal stratification. The dynamical constraint relates the tropopause potential temperature via a diffusive closure of baroclinic eddy fluxes to the surface potential temperature and its gradient, which are taken as given. Unlike baroclinic adjustment hypotheses, the proposed dynamical constraint does not presuppose the equilibration of baroclinic eddies to be weakly nonlinear. And unlike Juckes's and Emanuel's dynamical constraints, the proposed dynamical constraint neglects convective influences on the extratropical thermal stratification. Though

the effects of extratropical moist convection may not always be negligible, I regard it as foundational for any future general circulation theory to study how baroclinic eddies, in concert with radiative processes but in isolation from convection and other complicating factors such as surface topography and moisture effects, can determine the tropopause height and thermal stratification in the extratropics. The theoretical developments and analyses of simulations in this paper therefore focus on the mean state of a dry ideal-gas atmosphere with stationary and axisymmetric circulation statistics.

Section 2 derives a dynamical constraint on the extratropical tropopause height and thermal stratification by considerations of entropy fluxes, or isentropic mass fluxes, and their relation to baroclinic eddy fluxes of potential vorticity and surface potential temperature. The tropopause is taken as the upper boundary up to which significant isentropic mass fluxes originating at the surface extend, a view that leads to a balance condition for baroclinic eddy fluxes and, with the help of diffusive eddy flux closures, to the dynamical constraint. Section 3 describes an idealized GCM and a reference simulation with the idealized GCM, pointing to the possibility of an extratropical climate in which baroclinic eddy fluxes maintain a statically stable thermal stratification and, in interaction with large-scale diabatic processes, lead to the formation of a sharp tropopause. Section 4 summarizes a series of simulations with the idealized GCM that show that, across a wide range of atmospheric circulations, the proposed dynamical constraint describes the relation between tropopause and surface potential temperatures well. Section 5 shows that the dynamical constraint, derived for an idealized dry atmosphere, can also account for observed interannual variations of the tropopause height and thermal stratification in the extratropics of the earth's atmosphere. Section 6 discusses an implication of the dynamical constraint, namely, that if baroclinic eddies determine the tropopause height and thermal stratification, an atmosphere organizes itself into a state in which nonlinear interactions among the eddies are inhibited. Section 7 summarizes the conclusions. The appendix lists the notation and symbols used in this paper.

2. A dynamical constraint on the extratropical tropopause height and thermal stratification

a. Defining features of troposphere and tropopause

To develop a dynamical constraint on the extratropical tropopause height and thermal stratification, one needs a dynamically based definition of what constitutes the troposphere and tropopause. The existing ad hoc conventions of determining the tropopause, such as the World Meteorological Organization's convention or the convention of identifying the extratropical tropopause with an isoline of potential vorticity (Holton et al. 1995), provide adequate characterizations of the tropopause in

the present-day climate, but they may be inadequate in a changed climate. One needs a quantitative definition of the tropopause—or, equivalently, a quantitative distinction between troposphere and stratosphere—that is independent of the specific climatic state of the atmosphere and, preferably, is applicable to the Tropics and subtropics as well as to the extratropics.

Based on the view that the troposphere is the atmospheric layer within which the entropy received at the surface is redistributed, a quantitative distinction between troposphere and stratosphere can be derived from the entropy conservation law. In isentropic coordinates, entropy conservation is equivalent to mass conservation,

$$\partial_t \rho_\theta + \partial_x(\rho_\theta u) + \partial_y(\rho_\theta v) + \partial_\theta(\rho_\theta Q) = 0, \quad (1)$$

where horizontal derivatives are understood as derivatives along isentropes and $Q = D\theta/Dt$ denotes the material derivative of potential temperature θ.[1] The isentropic density $\rho_\theta = -(g^{-1}\partial_\theta p)\mathcal{H}(\theta - \theta_s)$ is the density in (x, y, θ) space ($\rho_\theta\, dx\, dy\, d\theta = \rho\, dx\, dy\, dz$ is a mass element), and the Heaviside step function $\mathcal{H}(\cdot)$ indicates that the isentropic density vanishes on isentropes "inside" the surface, that is, on isentropes with potential temperature θ less than the instantaneous surface potential temperature $\theta_s(x, y, t)$. Averaging the conservation law (1) yields

$$\partial_y(\overline{\rho}_\theta \overline{v}^*) + \partial_\theta(\overline{\rho}_\theta \overline{Q}^*) = 0, \quad (2)$$

where $\overline{(\cdot)}^* = \overline{(\rho_\theta \cdot)}/\overline{\rho}_\theta$ denotes the density-weighted mean associated with the temporal and zonal mean $\overline{(\cdot)}$ along isentropes. The conservation law (2) can be regarded as the mean conservation law for mass or, if multiplied by the specific entropy, as the mean conservation law for entropy.

In terms of the conservation law (2), the view of the troposphere as the atmospheric layer within which the entropy received at the surface is redistributed means that the divergence $\partial_y(\overline{\rho}_\theta \overline{v}^*)$ of isentropic mass fluxes originating at the surface is of much larger magnitude in the troposphere than in overlying atmospheric layers. Both in the extratropics and in the Tropics and subtropics of the earth's atmosphere, the absolute value of the divergence $\partial_y(\overline{\rho}_\theta \overline{v}^*)$ of the annual and zonal mean mass flux along isentropes drops by about two orders of magnitude across the tropopause, from values up to 10^{-4} kg K^{-1} m^{-2} s^{-1} in the troposphere to values on the order of 10^{-6} kg K^{-1} m^{-2} s^{-1} in the lower stratosphere.[2] Since the divergence of a mass flux indicates a rate of replacement of air masses, a large magnitude

of the divergence $\partial_y(\overline{\rho}_\theta \overline{v}^*)$ of isentropic mass fluxes originating at the surface implies a large rate at which air masses in isentropic layers are replaced with surface air. Dividing typical values of the isentropic density ($\overline{\rho}_\theta \sim 100$ kg m^{-2} K^{-1} in the troposphere and $\overline{\rho}_\theta \sim 20$ kg m^{-2} K^{-1} in the lower stratosphere) by the typical values of the divergence $\partial_y(\overline{\rho}_\theta \overline{v}^*)$ and assuming that the divergences of isentropic mass fluxes in the troposphere and in the lower stratosphere are due to entropy fluxes originating at the surface, one obtains typical values of the mean replacement times of air masses with surface air: on the order of 10 days in the troposphere and on the order of 1 year in the lower stratosphere, consistent with estimates of the "mean age" of air derived from tracer measurements (cf. Hall and Plumb 1994; Andrews et al. 2001). That is, as is well known, air masses in isentropic layers in the troposphere are replaced much more efficiently with surface air than are air masses in isentropic layers in the stratosphere.

Making no reference to specific dynamic mechanisms of entropy redistribution, the distinction of troposphere and stratosphere in terms of the divergence of isentropic mass fluxes allows for a consistent characterization of the troposphere and tropopause in the Tropics, subtropics, and extratropics.

To the extent that the entropy received at the surface and any additional entropy received in the interior troposphere are entirely redistributed within the troposphere and do not reach the stratosphere, the mass circulation formed by the mass flux along isentropes $\overline{\rho}_\theta \overline{v}^*$ and the mass flux across isentropes $\overline{\rho}_\theta \overline{Q}^*$ closes within the troposphere. That is, at each latitude, the mass flux $\overline{\rho}_\theta \overline{v}^*$ along isentropes integrated from a potential temperature $\theta_b(y)$ less than the lowest potential temperature that occurs at the latitude to the temporal and zonal mean potential temperature $\overline{\theta}_t(y)$ of the tropopause approximately vanishes:

$$\int_{\theta_b}^{\overline{\theta}_t} \overline{\rho}_\theta \overline{v}^* \, d\theta \approx 0. \quad (3)$$

This constraint on the mass flux along isentropes defines the tropopause potential temperature $\overline{\theta}_t$ as the potential temperature at which the streamfunction of the mass fluxes along and across isentropes closes approximately. (A quantitative version of this definition is given in section 4b.) For the present-day earth atmosphere, the tropopause potential temperature thus determined roughly agrees with the conventionally determined tropopause potential temperature (cf. Bartels et al. 1998, their Fig. 1).

To derive a dynamical constraint on the extratropical tropopause height and thermal stratification from the mass flux constraint (3), one needs to relate the extratropical mass flux along isentropes to eddy fluxes of adiabatically conserved quantities, and these eddy fluxes, via a turbulence closure, to the thermal stratification of the troposphere.

---

[1] For simplicity of notation, local Cartesian coordinates x and y are used as horizontal coordinates. Where numerical values of derivatives are given, however, they have been computed in spherical coordinates.

[2] The values are computed from National Centers for Environmental Prediction–National Center for Atmospheric Research (NCEP–NCAR) reanalysis data (Kalnay et al. 1996). They are consistent with the data, for example, of Yang et al. (1990, their Figs. 6 and 10).

b. Extratropical eddy fluxes and the mass flux along isentropes

In the extratropics, where the Rossby number is small, the isentropic mass flux $\overline{\rho}_\theta \overline{v}^*$ at each latitude is related to eddy fluxes of potential vorticity P and of surface potential temperature θ_s via the approximate balance condition [Schneider (2003); see also Held and Schneider (1999) and Tung (1986)]:

$$\int_{\theta_b}^{\theta_i} \overline{\rho}_\theta \overline{v}^* \, d\theta \approx -\int_{\theta_b}^{\theta_i} \frac{\overline{\rho_\theta \hat{v}\hat{P}}^*}{\overline{P}^*} \, d\theta - \overline{\rho}_\theta^0 \, \overline{\tilde{v}_s' \theta_s'}^s. \quad (4)$$

The upper limit of the integrations is an arbitrary potential temperature θ_i greater than the largest surface potential temperature that typically occurs at the latitude under consideration. The symbol $\overline{\rho}_\theta^0 = \overline{\rho}_\theta(y, \overline{\theta}_s)$ denotes the isentropic density at the temporal and zonal mean surface potential temperature $\overline{\theta}_s$, and

$$\tilde{v}_s' = f^{-1}\partial_x(M_s' - c_p\theta_s'),$$

with Montgomery streamfunction $M = c_pT + gz$ and with the subscript s marking surface quantities, denotes a balanced meridional velocity at the surface (approximately the geostrophic velocity). The temporal and zonal mean $\overline{(\cdot)}^s$ along the surface appears in addition to the temporal and zonal mean $\overline{(\cdot)}$ along isentropes and the associated density-weighted mean $\overline{(\cdot)}^*$. Hats denote fluctuations $(\hat{\cdot}) = (\cdot) - \overline{(\cdot)}^*$ about the density-weighted isentropic mean, and primes denote fluctuations $(\cdot)' = (\cdot) - \overline{(\cdot)}^s$ about the surface mean. On isentropes inside the surface, the isentropic density ρ_θ, the velocities u and v, and the relative vorticity component ζ_θ normal to isentropes vanish. Since the isentropic density vanishes, the contribution of isentropes inside the surface, for example, to the mean potential vorticity $\overline{P}^* = \overline{[\rho_\theta(f + \zeta_\theta)/\rho_\theta]}/\overline{\rho}_\theta$ involves the indefinite expression $(f + \zeta_\theta)\rho_\theta/\rho_\theta$. Implicit in the balance condition (4) is the convention that, inside the surface, $(f + \zeta_\theta)\rho_\theta/\rho_\theta = f + \zeta_\theta = f$, such that the mean potential vorticity can be written as $\overline{P}^* = (f + \overline{\zeta}_\theta)/\overline{\rho}_\theta$, even on isentropes that sometimes intersect the surface [see Schneider (2003) for details].

The balance condition (4) derives from the zonal momentum balance of isentropes. It states that the vertically integrated mass flux $\overline{\rho}_\theta \overline{v}^*$ along isentropes is approximately composed of a mass flux associated with the eddy flux $\overline{\hat{v}\hat{P}}^*$ of potential vorticity along isentropes, and a mass flux associated with the balanced eddy flux $\overline{\tilde{v}_s' \theta_s'}^s$ of surface potential temperature. Neglected in the balance condition (4) are the Ekman mass flux due to surface friction, terms of higher order in Rossby number, and terms containing eddy fluxes such as $\overline{\tilde{v}_s' \theta_s'^2}^s$ that involve higher moments of surface potential temperature fluctuations. Since the Ekman mass flux is primarily balanced by the convergence of eddy momentum fluxes in the upper troposphere, neglecting the Ekman mass

flux in the balance condition (4) is tantamount to neglecting the contribution of the eddy momentum flux convergence to the eddy flux of potential vorticity.

The assumption that eddies tend to homogenize quantities that are materially conserved in adiabatic and frictionless flows leads to a qualitative account of the extratropical mass flux along isentropes. Isentropes in two separate layers must be distinguished (Held and Schneider 1999; Schneider 2003).

First, the *interior atmosphere* at a latitude comprises isentropes $\theta \gtrsim \max(\theta_s)$ that, at that latitude, typically do not intersect the surface. The mass flux along isentropes in the interior atmosphere is associated with the eddy flux $\overline{\hat{v}\hat{P}}^*$ of potential vorticity. The meridional gradient $\partial_y \overline{P}^*$ of potential vorticity along isentropes is usually positive in the interior troposphere—because the planetary vorticity gradient β is positive, and because the isentropic density $\overline{\rho}_\theta$ usually decreases poleward along interior isentropes, such that, neglecting relative vorticity gradients, both factors contribute to a positive potential vorticity gradient

$$\partial_y \overline{P}^* \approx \partial_y\left(\frac{f}{\overline{\rho}_\theta}\right) = \frac{\beta}{\overline{\rho}_\theta} - f\frac{\partial_y \overline{\rho}_\theta}{\overline{\rho}_\theta^2}. \quad (5)$$

Downgradient mixing of potential vorticity hence leads to a southward eddy flux $\overline{\hat{v}\hat{P}}^*$, which implies a poleward contribution to the mass flux (4).

Second, the *surface layer* at a latitude comprises isentropes $\theta_b \leq \theta \leq \max(\theta_s)$ that, at that latitude, sometimes intersect the surface. The mass flux along isentropes in the surface layer is associated with the balanced eddy flux $\overline{\tilde{v}_s' \theta_s'}^s$ of surface potential temperature and with the eddy flux $\overline{\hat{v}\hat{P}}^*$ of potential vorticity. Mixing of surface potential temperature down the meridional gradient $\partial_y \overline{\theta}_s$ leads to a poleward eddy flux $\overline{\tilde{v}_s' \theta_s'}^s$, which implies an equatorward contribution to the mass flux (4). This equatorward mass flux can be augmented by a mass flux associated with the eddy flux $\overline{\hat{v}\hat{P}}^*$ of potential vorticity in the surface layer. Within the surface layer, the isentropic density $\overline{\rho}_\theta = \overline{\rho_\theta \mathcal{H}(\theta - \theta_s)}$ increases poleward along isentropes, primarily because the frequency with which the potential temperature θ of an isentrope is greater than the instantaneous surface potential temperature θ_s (i.e., the frequency with which the isentrope is above the surface) increases as one moves poleward along the isentrope. The isentropic-density gradient $\partial_y \overline{\rho}_\theta$ thus provides a negative contribution, $-f\partial_y \overline{\rho}_\theta/\overline{\rho}_\theta^2$, to the potential vorticity gradient (5). As one moves downward through the surface layer at constant latitude, this negative contribution to the potential vorticity gradient eventually dominates the positive contribution $\beta/\overline{\rho}_\theta$ of the planetary vorticity gradient β because the isentropic density $\overline{\rho}_\theta$ decreases to zero at the bottom of the surface layer. Downgradient mixing of potential vorticity hence can lead to a northward eddy flux $\overline{\hat{v}\hat{P}}^*$, which, similar to a poleward eddy

flux $\overline{v'_s\theta'}^s$ of surface potential temperature, implies an equatorward contribution to the mass flux (4).[3]

The constraint (3) on the mass flux along isentropes implies that the equatorward mass flux in the surface layer and the poleward mass flux in the interior atmosphere are in balance within the troposphere. Combining the mass flux constraint (3) with the balance condition (4) relating mass fluxes and eddy fluxes, one obtains a constraint on extratropical eddy fluxes:

$$\int_{\theta_b}^{\overline{\theta}_t} \frac{\overline{\rho_\theta \hat{v}\hat{P}}^*}{\overline{P}^*} \, d\theta \approx -\overline{\rho}_\theta^0 \, \overline{v'_s\theta'_s}^s. \qquad (6)$$

At each latitude, the vertically integrated mass flux associated with the eddy flux of potential vorticity approximately balances the vertically integrated mass flux associated with the balanced eddy flux of surface potential temperature. A similar constraint holds for quasigeostrophic eddy fluxes: if one neglects dissipation and the eddy momentum flux convergence (or, equivalently, the meridional wave activity flux divergence), the vertically integrated eddy flux of quasigeostrophic potential vorticity is proportional to the geostrophic eddy flux of potential temperature at the surface (see, e.g., Treguier et al. 1997). However, the mass flux associated with the eddy flux of potential vorticity in the surface layer has no counterpart in quasigeostrophic models of a continuously stratified atmosphere.

c. Diffusive closure of extratropical eddy fluxes

Going beyond the assumption that the meridional eddy fluxes of potential temperature along the surface and of potential vorticity along isentropes are directed downgradient, one can model the eddy fluxes as diffusive fluxes,

$$\overline{v'_s\theta'_s}^s \approx -D_s\partial_y\overline{\theta}_s \quad \text{and} \qquad (7a)$$

$$\overline{\hat{v}\hat{P}}^* \approx -D_i\partial_y\overline{P}^*, \qquad (7b)$$

with nonnegative eddy diffusivities D_s and D_i for surface potential temperature and for potential vorticity on isentropes. The eddy diffusivities can, and usually do, depend on the mean thermal stratification of the atmosphere and may vary with latitude on length scales that are large compared with typical eddy length scales. However, the precise form of the eddy diffusivities is irrelevant for the considerations that follow.

Modeling the meridional eddy fluxes in the extratropics as diffusive fluxes is justifiable because two conditions are approximately met (cf. Rhines and Holland 1979; Held 1999): to the extent that convective heating

is negligible, surface potential temperature and potential vorticity are nearly materially conserved on the time scales of extratropical eddies; and typical meridional length scales of the energy-containing baroclinic eddies in the earth's atmosphere (about 3500 km) are smaller than the planetary scales over which the mean surface potential temperature and the mean potential vorticity vary (about 10 000 km).[4] However, since the eddy length scales are not much smaller than the mean-flow length scales—in particular near the top of the surface layer, where the meridional potential vorticity gradient changes sign—the accuracy that can be expected of diffusive closures is limited [see Corrsin (1974) for estimates of how scale separation relates to the accuracy of diffusive closures].

d. Diffusive eddy flux closure and tropopause properties

With the diffusive closure (7b) of the eddy flux of potential vorticity as the point of departure, one can distinguish how different factors influence properties of the extratropical tropopause. If the troposphere is clearly distinguished from the stratosphere in that the bulk of the entropy received at the surface is redistributed within the troposphere but does not reach the stratosphere, the mass flux along isentropes in the interior atmosphere (cf. Tung 1986),

$$\overline{\rho}_\theta\overline{v}^* \approx -\frac{\overline{\rho_\theta\hat{v}\hat{P}}^*}{\overline{P}^*} \approx \frac{\overline{\rho}_\theta D_i\partial_y\overline{P}^*}{\overline{P}^*}, \qquad (8)$$

must decrease strongly across a sharp tropopause. Observational data show that kinematic eddy diffusivities generally do not vary strongly across the extratropical tropopause. The empirical eddy diffusivity $\tilde{D}_i = -\overline{\hat{v}\hat{P}}^*/\partial_y\overline{P}^*$ implied by the observed eddy flux and mean gradient of potential vorticity does not generally exhibit sharp variations across the extratropical tropopause, with the exception of stronger variations in the winter hemisphere in the vicinity of localized regions of strong baroclinicity, where the potential vorticity gradient is close to zero (Bartels et al. 1998). And Nakamura's (1996) effective diffusivity, a Lagrangian eddy diffusivity that quantifies mixing efficiency, exhibits a minimum near the subtropical tropopause, in the core of the subtropical jet, but it does not exhibit sharp variations across the extratropical tropopause (Haynes and Shuckburgh 2000). Observational data thus suggest that, unlike the subtropical tropopause, the extratropical tropopause cannot, as is

---

[3] See Held and Schneider (1999) and Schneider (2003) for more detailed discussions of the relation between isentropic mass fluxes and eddy fluxes of potential vorticity and surface potential temperature, including a discussion of how the presence of a mixed layer at the surface modifies the distribution of isentropic mass fluxes.

[4] Additionally, the distinction between the balanced (approximately geostrophic) meridional eddy flux of surface potential temperature appearing in the balance condition (6) and the actual meridional eddy flux of potential temperature near the surface can be neglected because meridional velocity fluctuations in baroclinic eddies are approximately geostrophic.

sometimes stated, be viewed as a mixing barrier, at least not in the sense that strong variations of kinematic mixing properties would in general define the tropopause. The strong decrease of the isentropic mass flux across the extratropical tropopause, and the concomitant large gradients of tracers such as nitrous oxide (see, e.g., Mahlman 1997), are not primarily due to a strong decrease of kinematic eddy diffusivities.

If the kinematic eddy diffusivity D_i does not vary strongly across the extratropical tropopause, the isentropic density $\overline{\rho}_\theta$, and with it the "isentropic dynamic eddy diffusivity" $\overline{\rho}_\theta D_i$, must decrease strongly for the isentropic mass flux to decrease strongly across the tropopause. The only other way for the isentropic mass flux (8) to decrease strongly across the tropopause would be through a strong decrease of the logarithmic potential vorticity gradient $\partial_y \overline{P}^* / \overline{P}^*$—a decrease that is not observed in the earth's atmosphere. In the observational data shown by Bartels et al. (1998, their Fig. 4) and in the simulations described in section 4, the empirical eddy diffusivity for potential vorticity typically decreases by about a factor of 2 across the extratropical tropopause, except in localized regions of strong baroclinicity, where the decrease can be greater. In contrast, the isentropic density typically decreases by about a factor of 4–5 across the tropopause, not only in localized regions of strong baroclinicity, but throughout the extratropics. The decrease of the isentropic density $\overline{\rho}_\theta \propto \rho/N^2$ by about a factor of 4–5 is consistent with the observed increase of the Brunt–Väisälä frequency N by about a factor of 2 (Peixoto and Oort 1992, chapter 7). The maximum of the potential vorticity gradient (5) at the tropopause implied by the strong decrease of the isentropic density is associated with a maximum of the eddy flux of potential vorticity at the tropopause (Bartels et al. 1998, their Fig. 3), consistent with the relatively weak variation of the eddy diffusivity across the tropopause. Nonetheless, the isentropic mass flux streamfunctions that Johnson (1989) and Bartels et al. (1998) obtained from observational data show that the mass flux associated with the maximum of the potential vorticity gradient at the tropopause is small compared with the mass flux in the interior troposphere. These data show, then, that it is the increase of the static stability that primarily accounts for the decrease of the isentropic mass flux across the extratropical tropopause.

e. A dynamical constraint on the extratropical tropopause height and thermal stratification

Substituting the diffusive closure (7) into the constraint (6) on the extratropical eddy fluxes yields

$$\int_{\theta_b}^{\overline{\theta}_t} \frac{\overline{\rho}_\theta D_i \partial_y \overline{P}^*}{\overline{P}^*} \, d\theta \approx -\overline{\rho}_\theta^0 D_s \partial_y \overline{\theta}_s. \qquad (9)$$

By a series of rough approximations, this constraint can

be brought into a form that relates the tropopause potential temperature to external parameters and to the surface potential temperature.

To the extent that the baroclinic eddies that effect the eddy fluxes of potential vorticity and surface potential temperature are vertically coherent within the troposphere, one can expect that, at each latitude, the eddy diffusivity D_i for potential vorticity exhibits no essential vertical structure within the troposphere (except in regions in which the potential vorticity gradient $\partial_y \overline{P}^*$ is close to zero); moreover, one can expect a vertical mean of the eddy diffusivity D_i for potential vorticity to be approximately equal to the eddy diffusivity D_s for surface potential temperature. This expectation of essentially barotropic mixing appears to be a plausible heuristic, whether the mixing is effected by waves or turbulence. For Rossby waves, the meridional group velocity is largest for barotropic waves; for fully developed turbulence, one would expect an inverse energy cascade to lead to barotropization of the energy-containing scales of the flow. To be sure, in quasigeostrophic theories, in which the thermal stratification and the tropopause height (or their correlatives) are fixed and unaffected by eddy fluxes, it is generally impossible to satisfy eddy-flux constraints such as the one [Eq. (9)] above with an eddy diffusivity for potential vorticity that is vertically constant and equal to the eddy diffusivity for surface potential temperature, unless the planetary vorticity gradient β can be neglected (Treguier et al. 1997; see also footnote 6); rather, given the tropopause height and thermal stratification, the vertical structure of the eddy diffusivities must be adjusted such that the eddy-flux constraints are satisfied (see, e.g., Smith and Vallis 2002). But if the tropopause height and thermal stratification, instead of being fixed, are determined by eddy fluxes, a different adjustment process is possible. The tropopause height and thermal stratification can adjust themselves such that the eddy flux constraint (9) is satisfied with an eddy diffusivity D_i for potential vorticity that exhibits no essential vertical structure within the troposphere and that, vertically averaged, is approximately equal to the eddy diffusivity D_s for surface potential temperature. This adjustment process is posited as determining the extratropical tropopause height and thermal stratification: if no vertical inhomogeneities are imposed, the tropopause height and thermal stratification adjust such that they are consistent with eddy fluxes whose kinematic mixing properties, reflected by the eddy diffusivities, exhibit no essential vertical inhomogeneities within the troposphere. The left-hand side of the constraint (9) can then be approximated by

$$\int_{\theta_b}^{\overline{\theta}_t} \frac{\overline{\rho}_\theta D_i \partial_y \overline{P}^*}{\overline{P}^*} \, d\theta \approx D_s \int_{\theta_b}^{\overline{\theta}_t} \frac{\overline{\rho}_\theta \partial_y \overline{P}^*}{\overline{P}^*} \, d\theta, \qquad (10)$$

and the constraint (9) becomes independent of the eddy diffusivities.

The integral (10) can be calculated using the small Rossby number approximation of the potential vorticity $\overline{P}^* \approx f/\overline{\rho}_\theta$ and the relation $\overline{\rho}_\theta = -g^{-1}\partial_\theta\overline{p}$ between isentropic density and pressure, with Lorenz's (1955) convention that the instantaneous pressure on isentropes inside the surface is equal to the surface pressure. One finds

$$\int_{\theta_b}^{\overline{\theta}_t} \frac{\overline{\rho}_\theta \partial_y \overline{P}^*}{\overline{P}^*} \, d\theta \approx \int_{\theta_b}^{\overline{\theta}_t} \left(\frac{\beta}{f}\overline{\rho}_\theta - \partial_y\overline{\rho}_\theta\right) d\theta$$

$$\approx \frac{\beta}{f}\frac{\overline{p}_s - \overline{p}_t}{g}, \qquad (11)$$

where $\overline{p}_s = \overline{p}(\theta_b)$ and $\overline{p}_t = \overline{p}(\overline{\theta}_t)$ denote the temporal and zonal mean pressure at the surface and at the tropopause. The boundary term $g^{-1}\partial_y\overline{p}\,|_{\theta_b}^{\overline{\theta}_t}$ of the integration of the isentropic-density gradient $\partial_y\overline{\rho}_\theta$ has been neglected. In the earth's atmosphere, the surface pressure gradient $\partial_y\overline{p}_s = \partial_y\overline{p}(\theta_b)$ is much smaller in absolute value than the scaled pressure difference $(\beta/f)(\overline{p}_s - \overline{p}_t)$ between surface and tropopause; the pressure gradient $\partial_y\overline{p}(\overline{\theta}_t)$ along isentropes at the tropopause (a measure of the slope of isentropes) is about an order of magnitude smaller in absolute value than the scaled pressure difference $(\beta/f)(\overline{p}_s - \overline{p}_t)$.[5] Neglecting this boundary term means that the part of the potential vorticity gradient that is associated with the isentropic-density gradient does not contribute to the integral (11). In terms of isentropic mass fluxes, neglecting the boundary term amounts to the approximation that, if the eddy diffusivity D_i for potential vorticity varies only weakly in the vertical, the mass fluxes associated with the contributions of the isentropic-density gradient to the potential vorticity gradient (which are of opposite sign in the surface layer and interior atmosphere) cancel upon vertical integration over the troposphere.

A further simplification of the constraint (9) results with the rough approximation

$$\overline{\rho}_\theta^0 \approx \frac{1}{g}\frac{\overline{p}_s - \overline{p}_t}{\overline{\theta}_t - \overline{\theta}_s} \qquad (12)$$

for the isentropic density at the mean surface potential temperature. This approximation generally is not very accurate. Since the isentropic density $\overline{\rho}_\theta^0$ at the mean surface potential temperature is the isentropic density

at the center of the surface layer, where the mean pressure is smaller than the mean surface pressure, one expects the approximation (12) to overestimate the isentropic density $\overline{\rho}_\theta^0$. However, the relation between the isentropic density $\overline{\rho}_\theta^0$ and the discrete approximation $g^{-1}(\overline{p}_s - \overline{p}_t)/(\overline{\theta}_t - \overline{\theta}_s)$ is complex. The variations with latitude of the extratropical isentropic density $\overline{\rho}_\theta^0$ at the mean surface potential temperature are considerably greater than those of the discrete approximation $g^{-1}(\overline{p}_s - \overline{p}_t)/(\overline{\theta}_t - \overline{\theta}_s)$. In wintertime polar inversions, according to NCEP–NCAR reanalysis data, the Brunt–Väisälä frequency N near the surface can be about a factor of 2 greater than in the midtroposphere, resulting in an isentropic density $\overline{\rho}_\theta^0 \propto N^{-2}$ at the mean surface potential temperature that is about a factor of 4 smaller than the discrete approximation (12) would suggest. Nonetheless, when multiplied by the surface potential temperature gradient $\partial_y\overline{\theta}_s$, as on the right-hand side of the constraint (9), and averaged over the extratropics, the approximation (12) entails an error of 20%–45% according to NCEP–NCAR reanalysis data. The simulations analyzed in section 4e moreover indicate that in the presence of strong surface inversions, what are denoted as surface quantities on the right-hand side of the constraint (9) should be interpreted as quantities at the top of the boundary layer. If the isentropic density $\overline{\rho}_\theta^0$ is interpreted as a quantity at the top of the boundary layer, the approximation (12) appears to be relatively good. For a dynamical constraint on the tropopause height and thermal stratification averaged over the extratropics, then, the approximation (12) appears to be justifiable, at least as a scaling estimate.

With the approximations (9)–(12), one obtains a dynamical constraint that relates the tropopause potential temperature to external parameters and to the surface potential temperature and its gradient:

$$\overline{\theta}_t - \overline{\theta}_s \approx -\frac{f}{\beta}\partial_y\overline{\theta}_s. \qquad (13)$$

This dynamical constraint states that the potential temperature difference $\overline{\theta}_t - \overline{\theta}_s$ between tropopause and surface is approximately equal to minus the surface potential temperature gradient multiplied by $f/\beta = a\tan(\phi)$, where a is the planet radius and ϕ is latitude. If the surface potential temperature gradient in midlatitudes [where $\tan(\phi) \approx 1$] multiplied by the planet radius a can be taken as a measure of the equator-to-pole surface potential temperature difference, the dynamical constraint (13) states that the potential temperature difference between tropopause and surface in midlatitudes is approximately equal to the surface potential temperature difference between equator and pole, as is the case in the earth's atmosphere.

Since the dynamical constraint is based on diffusive closures of eddy fluxes, and given the roughness of the approximations made, the dynamical constraint (13) can only be expected to hold on meridional scales that are

---

[5] Using $\partial_y p|_\theta = -(\partial_p\theta)^{-1}\partial_y\theta|_p = pg^2/(RN^2T^2)\partial_yT|_p$ and values typical of the midlatitude tropopause [$p \approx 250$ hPa, $T \approx 220$ K, $N \approx 1.9 \times 10^{-2}$ s^{-1} (corresponding to a temperature lapse rate of 2 K km^{-1}), and $\partial_yT|_p \approx \pm 3 \times 10^{-6}$ K m^{-1} (see Peixoto and Oort 1992, chapter 7)], one finds for the scaled isentropic pressure gradient $|(f/\beta)\partial_y\overline{p}(\overline{\theta}_t)| \approx a|\partial_y\overline{p}(\overline{\theta}_t)| \approx 90$ hPa. In midlatitudes, the scaled pressure gradient $(f/\beta)\partial_y\overline{p}(\overline{\theta}_t)$ along isentropes at the tropopause is thus about an order of magnitude smaller in absolute value than the pressure difference $\overline{p}_s - \overline{p}_t$.

large compared with typical eddy length scales. In an earth-like atmosphere in which eddy length scales are not much smaller than the planetary scale, the dynamical constraint (13) can therefore only be expected to hold for extratropical averages.

The dynamical constraint derived from the baroclinic adjustment hypothesis that the quasigeostrophic potential vorticity gradient vanishes in the interior atmosphere has a form similar to that of the present constraint (13), with the potential temperature gradient along pressure surfaces in the midtroposphere in place of the surface potential temperature gradient (cf. Lindzen and Farrell 1980; Held 1982). Considerations of the dynamics of quasigeostrophic models, however, would not lead to the constraint (13). In quasigeostrophic theory, the potential vorticity flux along isentropes is represented as a quasigeostrophic potential vorticity flux along fixed horizontal planes (Charney and Stern 1962). But since the horizontal planes in quasigeostrophic theory are fixed, whereas a surface-layer isentrope at a given latitude lies sometimes inside the surface, sometimes above the surface, the quasigeostrophic potential vorticity balance averaged along near-surface horizontal planes differs fundamentally from the potential vorticity balance averaged along surface-layer isentropes. Layer models such as Phillips's (1954) two-layer model can represent the potential vorticity fluxes and associated mass fluxes in isentropic layers (or in the surface layer and interior atmosphere), but since they lack a representation of the fact that surface-layer isentropes sometimes lie inside the surface, they cannot represent the isentropic mass flux associated with the balanced eddy flux of surface potential temperature—the contribution to the isentropic mass flux that gives rise to the appearance of the surface potential temperature gradient in the constraint (13). Continuously stratified models such as Charney's (1947) model can represent the potential vorticity fluxes along interior isentropes, the balanced eddy flux of surface potential temperature, and the associated mass fluxes, but since they lack a representation of the fact that surface-layer isentropes sometimes lie above the surface, they cannot represent the isentropic mass flux associated with the eddy flux of potential vorticity in the surface layer. In the mean quasigeostrophic potential vorticity balance near the surface, there appears either the geostrophic eddy flux of surface potential temperature (in continuously stratified models), or an eddy flux of potential vorticity (in layer models) that can be interpreted as a flux in the isentropic surface layer; however, both eddy flux components do not appear simultaneously in quasigeostrophic models [see Schneider (2003) for details]. Yet it is the simultaneous appearance of both eddy flux components in the mean potential vorticity balance of surface-layer isentropes that makes it possible to postulate that the eddy diffusivity for potential vorticity exhibits no essential vertical structure within the troposphere and is, vertically averaged, approximately equal to the eddy diffusivity for surface potential temperature.[6] Considerations of the dynamics of isentropic layers combine elements of quasigeostrophic layer models and continuously stratified models and were essential for the derivation of the dynamical constraint (13)—similar to quasigeostrophic theory, with the approximation that the Rossby number vanishes, but different from quasigeostrophic theory, without the approximation that fluctuations of the static stability (or isentropic density) about a fixed reference profile be small, an approximation that would be inadequate for surface-layer isentropes.

The dynamical constraint (13) can be combined with a radiative constraint to obtain a closed theory of the tropopause height and thermal stratification in the extratropics. In addition to the postulate that the eddy diffusivity D_i for potential vorticity exhibits no essential vertical structure within the troposphere and is, vertically averaged, approximately equal to the eddy diffusivity D_s for surface potential temperature, the dynamical constraint is based on several premises: (i) baroclinic eddies dominate the entropy transport and transport entropy efficiently enough to maintain the static stability of the extratropics, while convective entropy transport can be neglected; (ii) turbulent fluxes due to baroclinic eddies, in interaction with large-scale diabatic processes, can lead to the formation of a distinct troposphere separated from a stratosphere by a tropopause; and (iii) the extratropical tropopause height and thermal stratification are set locally by extratropical processes and do not depend on tropical processes. By means of simulations with an idealized GCM, it was investigated whether these premises are plausible and to what degree

---

[6] An argument put forth by I. Held (2002, personal communication) shows in more detail how quasigeostrophic dynamical constraints on the thermal stratification differ from the present constraint. Neglecting eddy momentum fluxes and taking the upper boundary at infinity, the quasigeostrophic counterpart of the balance condition (6) is

$$\int_0^\infty \frac{\rho_0 \overline{v_g' q'}^z}{f_0}\, dz \approx -\rho_0 \frac{\overline{v_g' \theta'}^z}{\partial_z \theta_0}\bigg|_{z=0},$$

where v_g is the geostrophic meridional velocity, q is the quasigeostrophic potential vorticity, the subscript 0 marks reference values and profiles, $\overline{(\cdot)}^z$ denotes a temporal and zonal mean along horizontal planes, and $(\cdot)' = (\cdot) - \overline{(\cdot)}^z$ denotes fluctuations about this mean. Substituting diffusive eddy flux closures with an eddy diffusivity $D(z)$ for potential vorticity that is, at the surface ($z = 0$), equal to the eddy diffusivity for surface potential temperature (cf. Treguier et al. 1997), neglecting the relative vorticity gradient in the potential vorticity gradient $\partial_y \overline{q}^z \approx \beta + f_0 \rho_0^{-1} \partial_z (\rho_0 \partial_y \overline{\theta}^z / \partial_z \theta_0)$, and integrating the left-hand side by parts yields

$$\int_0^\infty \rho_0 \left(D \frac{\beta}{f_0} - \partial_z D \frac{\partial_y \overline{\theta}^z}{\partial_z \theta_0} \right) dz \approx 0.$$

Unlike in the more general case (9), the boundary term of the integration by parts cancels the term involving the surface potential temperature gradient on the right-hand side. This relation shows that the surface potential temperature gradient generally does not appear in quasigeostrophic constraints on the thermal stratification and that the eddy diffusivity for quasigeostrophic potential vorticity can only be constant with height ($\partial_z D = 0$) if the planetary vorticity gradient β is negligible.

the dynamical constraint (13) holds if circulation parameters such as the planetary angular velocity and the differential heating of the surface are varied.

3. An idealized general circulation model

The idealized GCM used is a primitive-equation model in which the spherical lower boundary has no topography, quadratic damping of near-surface winds mimics turbulent dissipation in the planetary boundary layer, and Newtonian relaxation of temperatures toward a radiative equilibrium state represents diabatic processes. Vertical diffusion and convective adjustment are not taken into account in the model, with the exception that, in a narrow region around the equator, relaxation of temperatures toward a moist pseudoadiabat mimics dynamic heating due to moist convection. What distinguishes this model from similar idealized GCMs with Newtonian temperature relaxation is that the radiative equilibrium state toward which temperatures are relaxed is, in the extratropics, statically unstable, in contrast to the statically stable radiative–convective equilibrium states used in other idealized GCMs (e.g., James and Gray 1986; Held and Suarez 1994; Haynes et al. 2001). Since the model does not contain a representation of convective adjustment, only the turbulent entropy transport due to baroclinic eddies (possibly augmented by convective entropy transport on the grid scale) can maintain the static stability of the model extratropics. Hence, this idealized GCM is well suited for studying to what extent and how turbulent fluxes due to baroclinic eddies, in interaction with diabatic processes, can maintain the thermal stratification of a dry atmosphere and can contribute to the formation of an extratropical tropopause.

a. Dynamical core

The dynamical core of the idealized GCM is a hydrostatic spectral transform model in Bourke's (1974) vorticity–divergence form, with semi-implicit time differencing and a vertical σ coordinate (Durran 1999, chapter 7.6). The spectral truncation is triangular, and most simulations used T42 resolution (for an exception, see section 4a). The vertical discretization is based on a centered difference scheme, with 30 unequally spaced σ levels affording a relatively high vertical resolution throughout the troposphere that forms in the model (6 σ levels below $\sigma = 0.8$ and 17 σ levels below $\sigma = 0.2$). Subgrid-scale dissipation is represented by ∇^8 hyperdiffusion in the vorticity, divergence, and temperature equations. The dynamical core of the idealized GCM is identical with the spectral dynamical core described by Held and Suarez (1994). Further numerical specifications can be taken from Held and Suarez's description.

TABLE 1. Parameters of the reference simulation.

Planet and fluid	
Planet radius	$a = 6.371 \times 10^6$ m
Planetary angular velocity	$\Omega = 7.292 \times 10^{-5}$ s^{-1}
Specific heat at constant pressure	$c_p = 1004.6$ J kg^{-1} K^{-1}
Gas constant	$R = 286.9$ J kg^{-1} K^{-1}
Mean surface pressure	$p_0 = 1000$ hPa
Surface drag	
Frictional wavenumber	$k_d^0 = 0.7 \times 10^{-5}$ m^{-1}
Extent of "planetary boundary layer"	$\sigma_b = 0.85$
Diabatic processes	
Mean surface temperature	$\overline{T}_s^e = 300$ K
Equator-to-pole temperature difference	$\Delta_h = 60$ K
Skin temperature	$T_t^e = 200$ K
Scale height ratio H_p/H_a	$\alpha = 3.5$
Rescaling factor of pseudoadiabatic lapse rate	$\gamma = 1$
"Radiative" relaxation time in interior	$\tau_i = 50$ days
"Radiative" relaxation time near surace	$\tau_s = 7$ days
"Convective" relaxation time	$\tau_c = 4$ days

b. Surface drag

Quadratic damping

$$\frac{\partial \mathbf{v}}{\partial t} = \cdots - k_d(\sigma)\|\mathbf{v}\|\mathbf{v} \quad (14)$$

of the horizontal winds $\mathbf{v}$ near the surface mimics turbulent dissipation in the planetary boundary layer. The frictional wavenumber

$$k_d(\sigma) = k_d^0 \max\left(0, \frac{\sigma - \sigma_b}{1 - \sigma_b}\right)$$

is nonzero near the surface, in σ levels with $\sigma > \sigma_b = 0.85$. The frictional wavenumber decreases linearly in σ from $k_d = k_d^0$ at the surface ($\sigma = 1$) to $k_d = 0$ in σ levels above $\sigma = \sigma_b$. The frictional wavenumber k_d^0 at the surface is one of the parameters that were varied to investigate their influence on the extratropical tropopause height and thermal stratification; in the simulation referred to as the reference simulation (see Table 1), it was set to $k_d^0 = 0.7 \times 10^{-5}$ m^{-1}.

Aside from the ∇^8 hyperdiffusion representing subgrid-scale dissipation, the quadratic damping of near-surface winds is the only frictional process in the idealized GCM.

c. Diabatic processes

Diabatic processes are represented by Newtonian relaxation of temperatures T toward a zonally symmetric radiative equilibrium temperature T^e and, in a narrow region around the equator, toward a moist pseudoadiabat T^m:

$$\frac{\partial T}{\partial t} = \cdots - \frac{T - T^e(\phi, p)}{\tau_r(\phi, \sigma)} - w(\phi)\frac{T - T^m(p)}{\tau_c}. \quad (15)$$

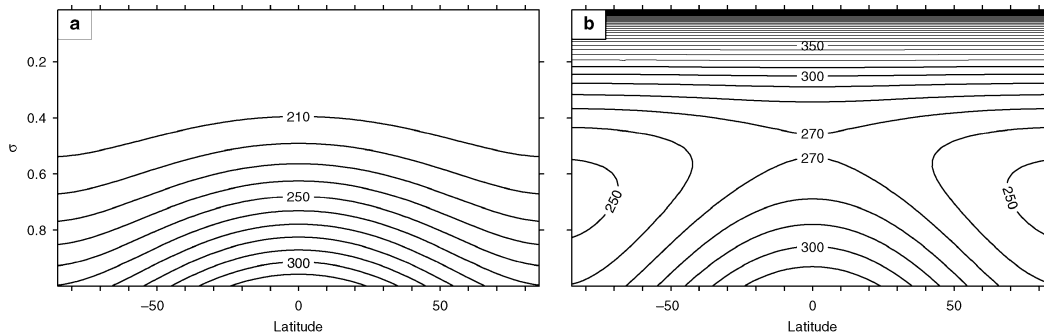The radiative equilibrium temperature $T^e(\phi, p)$, a func-

FIG. 1. (a) Temperature (K) and (b) potential temperature (K) in radiative equilibrium of the reference simulation.

tion of latitude ϕ and pressure p, is the radiative equilibrium temperature of a semigray atmosphere (Weaver and Ramanathan 1995). Temperatures are relaxed toward this radiative equilibrium temperature on a "radiative" time scale $\tau_r(\phi, \sigma)$ that depends on latitude ϕ and σ level. In a narrow region around the equator in which the weight function $w(\phi)$ has nonzero amplitude, temperatures are relaxed toward the temperature $T^m(p)$ of a moist pseudoadiabat on the "convective" time scale τ_c.

1) RELAXATION TOWARD RADIATIVE EQUILIBRIUM OF SEMIGRAY ATMOSPHERE

The surface air temperature in radiative equilibrium is specified as a function of latitude ϕ as

$$T_s^e(\phi) = \overline{T}_s^e + \Delta_h\left(\frac{1}{3} - \sin^2\phi\right),$$

where $\overline{T}_s^e = 300$ K is the global-mean surface temperature. The equator-to-pole temperature difference Δ_h in radiative equilibrium is one of the parameters that were varied; in the reference simulation, it was set to $\Delta_h = 60$ K.

The latitude–pressure dependence of the radiative equilibrium temperature is given by

$$T^e(\phi, p) = T_t^e\left[1 + d_0(\phi)\left(\frac{p}{p_0}\right)^\alpha\right]^{1/4}. \quad (16)$$

The skin temperature T_t^e at the top of the atmosphere ($p = 0$) is one of the parameters that were varied; in the reference simulation, it was set to $T_t^e = 200$ K. The constant $p_0 = 1000$ hPa is a reference surface pressure, and the exponent $\alpha = 3.5$ controls the lapse rate of the radiative equilibrium state. The requirement that for $p = p_0$ the radiative equilibrium temperature $T^e(\phi, p_0)$ match the radiative equilibrium temperature $T_s^e(\phi)$ at the surface yields

$$d_0(\phi) = \left[\frac{T_s^e(\phi)}{T_t^e}\right]^4 - 1 \quad (17)$$

for the function that controls the latitude dependence of the radiative equilibrium temperature (16).

Figure 1 shows the radiative equilibrium temperature and the associated potential temperature for the parameters of the reference simulation. It can be seen that the temperature gradient is largest at the surface and decreases to zero at the top of the atmosphere. The stratification of the radiative equilibrium state is statically unstable below $\sigma \approx 0.4$ and statically stable above that level, with a smooth transition between static stability and static instability. The statically unstable radiative equilibrium stratification in this model contrasts with the statically stable radiative equilibrium stratification used in other idealized GCMs, such as those used by Held and Suarez (1994) and Haynes et al. (2001).

The temperature T^e is the radiative equilibrium temperature of a semigray atmosphere, that is, of an atmosphere transparent to solar radiation and gray for infrared radiation (Weaver and Ramanathan 1995). Suppose the optical depth d of a semigray atmosphere decreases exponentially with altitude z so that $d = d_0 \exp(-z/H_a)$, where d_0 is the optical thickness of the atmosphere and H_a is the partial-pressure scale height of the principal infrared absorber (water vapor in the earth's atmosphere). If pressure decreases likewise exponentially with altitude, $p = p_0 \exp(-z/H_p)$ with pressure scale height H_p, the optical depth can be written as a function of pressure as

$$d = d_0\left(\frac{p}{p_0}\right)^\alpha,$$

where $\alpha = H_p/H_a$ is the ratio of the pressure scale height to the partial-pressure scale height of the infrared absorber. The function $d(\phi, p) = d_0(\phi)(p/p_0)^\alpha$ in the radiative equilibrium temperature (16) can thus be viewed as an optical depth that depends on latitude and pressure. Indeed, the radiative equilibrium temperature (16) is, up to constants, an equilibrium solution of the two-stream equations for a semigray atmosphere, with the function $d_0(\phi)(p/p_0)^\alpha$ playing the role of an optical depth (cf. Goody and Yung 1989, chapter 9.2). The choice of the exponent $\alpha = 3.5$ in the radiative equilibrium temper-

ature (16) is motivated by this correspondence between the radiative equilibrium temperature (16) and the radiative equilibrium temperature of a semigray atmosphere: in the earth's atmosphere, the ratio of the pressure scale height to the scale height of water vapor pressure is roughly $H_p/H_a \approx 7 \text{ km}/2 \text{ km} = 3.5$. However, the correspondence between radiative properties of the earth's atmosphere on the one hand and the radiative equilibrium temperatures of the idealized GCM and of a semigray atmosphere on the other hand is incomplete. For example, the latitude dependence of the optical thickness (17) is not motivated by the actual distribution of infrared absorbers in the earth's atmosphere, but by the desire to specify in radiative equilibrium both a surface air temperature with nonzero meridional gradient and a skin temperature with zero meridional gradient.

Temperatures are relaxed toward the radiative equilibrium temperature T^e on the "radiative" time scale $\tau_r(\phi, \sigma)$, which is a function of latitude ϕ and σ level with

$$\tau_r^{-1}(\phi, \sigma) = \tau_i^{-1} + (\tau_s^{-1} - \tau_i^{-1}) \max\left(0, \frac{\sigma - \sigma_b}{1 - \sigma_b}\right) \cos^8 \phi.$$

(18)

In σ levels above $\sigma = \sigma_b = 0.85$, the relaxation time scale is $\tau_r(\phi, \sigma \leq \sigma_b) = \tau_i = 50$ days. In σ levels below $\sigma = \sigma_b$, the relaxation time scale decreases toward the surface and, along the surface, toward the equator, taking the value $\tau_r(\phi = 0, \sigma = 1) = \tau_s \leq \tau_i$ at the equator. The near-surface relaxation time scale τ_s is one of the parameters that were varied; in the reference simulation, it was set to $\tau_s = 7$ days.

2) RELAXATION TOWARD MOIST PSEUDOADIABAT

The weight function

$$w(\phi) = 1 - \tanh\left(\frac{\sin^2 \phi}{\sin^2 \phi_t}\right), \qquad \phi_t = 6°,$$

determines the meridional extent of the region in which temperatures are relaxed toward a moist pseudoadiabat $T^m(p)$. The weight function decays steeply from $w(0) = 1$ at the equator to zero away from the equator. In the narrow region around the equator ($|\phi| \lesssim 6°$) in which the weight function has significant amplitude, temperatures are relaxed toward the moist pseudoadiabatic temperature

$$T^m(p) = T_s + \gamma \int_{p_s}^{p} \Gamma_m(p') \, dp' \qquad (19)$$

obtained by columnwise vertical integration of the moist pseudoadiabatic lapse rate $\Gamma_m(p)$ with respect to pressure decreases (cf. Emanuel 1994, chapter 4.7). The dimensionless factor γ rescales the pseudoadiabatic lapse rate Γ_m; the rescaling factor was set to $\gamma = 1$ in the reference

simulation and was varied to examine possible dependencies of the extratropical tropopause height and thermal stratification on the tropical thermal stratification. The instantaneous surface temperature T_s and surface pressure p_s provide the lower boundary conditions for the vertical integration of the pressure lapse rate. Above the level of neutral buoyancy, at which the temperature $T^m(p)$ of the moist pseudoadiabat is equal to the instantaneous temperature T, the temperature of the moist pseudoadiabat is set equal to the instantaneous temperature, so that the "convective" heating $- [T - T^m(p)]/\tau_c$ vanishes.

Equatorial temperatures are relaxed toward the moist pseudoadiabat $T^m(p)$ on the "convective" time scale $\tau_c = 4$ days.

d. Climate of a reference simulation

As a baseline for comparisons of simulations with different parameters, a reference simulation was performed in which the parameters were chosen such that the simulated large-scale circulation resembles that of the earth's atmosphere. Table 1 lists the values of the parameters in the reference simulation. The planet radius and the angular velocity are those of the earth, and the thermodynamic properties of the simulated fluid are those of dry air.

The simulation was started from an isothermal rest state with superimposed small random perturbations. After a spinup time of 800 simulated days, circulation statistics were computed from another 1200 simulated days in which flow fields were sampled 5 times per day. Since the forcing and the dissipation in the idealized GCM are hemispherically symmetric, the circulation statistics are, up to sampling error, likewise hemispherically symmetric. To reduce the sampling error in the circulation statistics, the simulated statistics of the two hemispheres were averaged, thereby enforcing symmetry of the plotted fields.

Figure 2 shows the streamfunction Ψ of the mean mass flux $(\overline{\rho}_\theta \overline{v}^*, \overline{\rho}_\theta \overline{Q}^*)$ in the dynamical equilibrium that develops in the reference simulation. The mass fluxes along isentropes and across isentropes are the derivatives

$$\overline{\rho}_\theta \overline{v}^* = \frac{1}{2\pi a \cos(\phi)} \partial_\theta \Psi \quad \text{and}$$

$$\overline{\rho}_\theta \overline{Q}^* = -\frac{1}{2\pi a \cos(\phi)} \partial_y \Psi$$

of the streamfunction $\Psi(y, \theta)$. Figure 2 shows that, as discussed in section 2b, equatorward mass flux along isentropes predominates in the surface layer, demarcated approximately by the 5% and 95% isolines of the cumulative distribution of surface potential temperatures; poleward mass flux along isentropes predominates in the interior troposphere. Upward and downward mass fluxes across isentropes, corresponding to diabatic heating and cooling, close the mass circulation. Figure 2
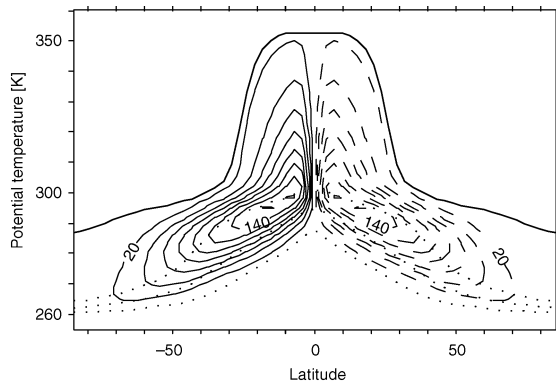
FIG. 2. Mass flux streamfunction ψ (10^9 kg s^{-1}) in the reference simulation (solid lines, counterclockwise rotation; dashed lines, clockwise rotation). The dotted lines represent the 5%, 50%, and 95% isolines of the cumulative distribution of surface potential temperatures. The thick line marks the tropopause, determined as the potential temperature $\overline{\theta}_t(y)$ in the interior atmosphere at which the absolute value of the streamfunction $|\Psi(y, \theta)|$ amounts to 10% of the maximum value $\max_\theta |\Psi(y, \theta)|$.

shows that the atmosphere of the idealized GCM is heated near the surface and in the Tropics, in the region in which temperatures are relaxed toward a moist pseudoadiabat; elsewhere, the atmosphere is cooled in the mean. There are no significant entropy sources in the interior atmosphere of the idealized GCM except in the Tropics, and so the statement that the troposphere is the layer of the atmosphere within which the entropy received at the surface is redistributed means that the circulation of mass along and across isentropes closes within the troposphere. Provided $\Psi = 0$ is chosen as the lower boundary condition on the streamfunction Ψ, the constraint (3) on the mass flux along isentropes implies that the mean tropopause potential temperature $\overline{\theta}_t(y)$ is a streamfunction envelope along which $\Psi(y, \overline{\theta}_t) \approx 0$. The tropopause plotted in Fig. 2 is determined as such an envelope of the streamfunction (see section 4b for details). As in the earth's atmosphere, the tropopause marks a transition between a troposphere in which the absolute value of the divergence $\partial_y(\overline{\rho}_\theta \overline{v}^*)$ of the mean mass flux along isentropes is on the order of

10^{-4} kg K^{-1} m^{-2} s^{-1}, and a stratosphere in which the absolute value of this divergence is significantly smaller, on the order of or less than 10^{-6} kg K^{-1} m^{-2} s^{-1}. The transition between troposphere and stratosphere is sharp in the extratropics and more gradual in the Tropics (cf. Fig. 5 below).

Figure 3 shows the simulated mean temperature and mean potential temperature. In the dynamical equilibrium that develops in the simulation, baroclinic eddies transport entropy poleward and upward, such that the mean meridional gradient of the surface temperature is reduced compared with the radiative equilibrium gradient (cf. Fig. 1). At the surface near the equator, a shallow statically unstable layer forms; this unrealistic feature of the simulation is unlikely to have a significant impact on the examined properties of the large-scale circulation. In the extratropics, although the radiative equilibrium state toward which temperatures are relaxed is statically unstable (Fig. 1b), the turbulent entropy transport due to baroclinic eddies is efficient enough to maintain a dynamical equilibrium that is in the mean, though not at every instant, statically stable (Fig. 3b). Less than 5% of the vertical entropy flux in the extratropics occurs at zonal wavenumbers greater than 20, which means that, if convective entropy transport on the grid scale contributes to the entropy transport at all, it must be coupled to the large-scale eddies and so is difficult to distinguish from them. With the caveat that grid-scale convective entropy fluxes coupled to baroclinic eddies may contribute to the entropy transport, the facts that the idealized GCM does not contain a representation of extratropical convective adjustment and that the extratropics are statically stable imply that, in this simulation, baroclinic eddies transport entropy efficiently enough to maintain the static stability of the extratropics.

At each latitude, the tropopause plotted in Fig. 3b indicates the mean σ level of the isentrope with potential temperature equal to the tropopause potential temperature $\overline{\theta}_t(y)$ plotted in Fig. 2. Figure 3b shows that, in accordance with the reasoning of section 2d, the extratropical tropopause marks a transition between a tro-
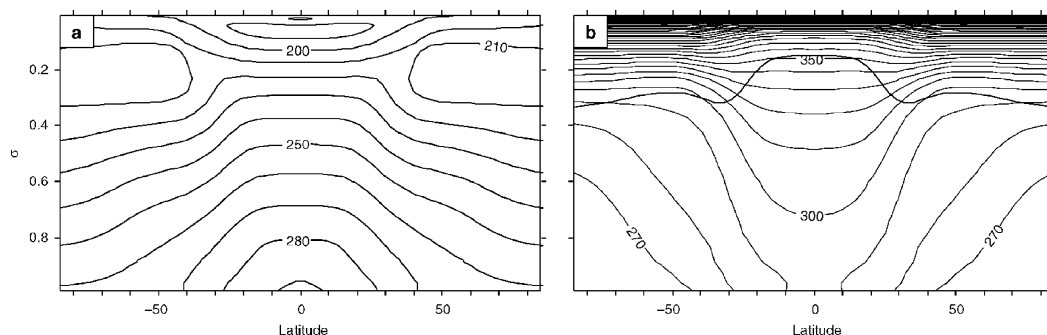

FIG. 3. (a) Mean temperature (K) and (b) potential temperature (K) in the reference simulation. The thick line in (b) marks the tropopause.

posphere with high isentropic density (low static stability) and a stratosphere with low isentropic density (high static stability). The Brunt–Väisälä frequency increases from 1.0×10^{-2} s^{-1} in the interior of the extratropical troposphere to 2.2×10^{-2} s^{-1} in the lower stratosphere—an increase similar to that observed in the earth's atmosphere.

The extratropical tropopause is also recognizable in instantaneous flow fields. Figure 4 shows a typical instantaneous potential vorticity field on the 298-K isentrope in the dynamical equilibrium of the reference simulation. A sharp increase of the static stability or decrease of the isentropic density ρ_θ shows up in the potential vorticity field $P = (f + \zeta_\theta)/\rho_\theta$ on isentropes that intersect the tropopause as a region of large meridional gradients. The tropopause, roughly coinciding with the ± 2 PVU isolines[7] of potential vorticity (cf. Holton et al. 1995), is clearly recognizable as the undulating region of large meridional potential vorticity gradients. Breaking of potential vorticity contours is seen on the entire isentrope, with filamentation of contours most clearly seen in the subtropics, where Rossby waves encounter their critical layers. The potential vorticity mixing that these processes entail is what is modeled with the diffusive eddy flux closure (7b).

That in the idealized GCM a well-defined extratropical tropopause forms without convective adjustment indicates that, in this model as in the model of Haynes et al. (2001), the extratropical tropopause forms through an interaction between large-scale diabatic processes and turbulent fluxes due to baroclinic eddies. The reference simulation points to the possibility of a climate in which premises (i) and (ii) of section 2e, assigning central importance to baroclinic eddy fluxes, hold.

4. Test of dynamical constraint with idealized GCM

a. Variation of parameters

The dynamical constraint (13) was tested in simulations with the idealized GCM with different values of some of the model parameters that influence the extratropical tropopause height and thermal stratification. The model parameters that were varied are listed in the first column of Table 2.

Simulations were carried out in which one parameter at a time was set to a different value than in the reference simulation. Only in the simulation with angular velocity $\Omega = 4\Omega^*$ (the asterisk denotes the reference parameter value listed in Table 1) were the angular velocity Ω, the skin temperature T_t^e, and the equator-to-pole temperature difference Δ_h varied simultaneously, for with an increased angular velocity $\Omega = 4\Omega^*$ and with reference values for the other parameters, the simulated stratifi-

---

[7] Potential vorticity is measured in potential vorticity units with 1 PVU = 10^{-6} K m^2 kg^{-1} s^{-1} (Hoskins et al. 1985).
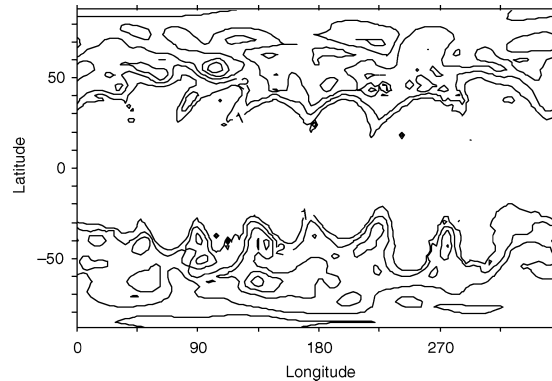

FIG. 4. An instantaneous potential vorticity field (contour interval is 1 PVU) on the 298-K isentrope.

cation turned out to be statically unstable. A statically stable stratification for $\Omega = 4\Omega^*$ was obtained by raising the skin temperature to $T_t^e = 225$ K and increasing the equator-to-pole temperature difference to $\Delta_h = 120$ K, thereby increasing the baroclinicity of the thermal forcing.

All simulations were run with the same vertical resolution of 30 σ levels. The horizontal resolution was T42 for all simulations except for the one with quadrupled angular velocity $\Omega = 4\Omega^*$, for which the horizontal resolution was increased to T63 to ensure that the smaller baroclinic eddies were resolved. Each simulation was spun up for at least 200 days from a circulation state for a point nearby in parameter space (a day referring to 86 400s, independently of the angular velocity Ω). Circulation statistics were sampled 5 times per day over another 400 simulated days. For the higher-resolution simulation (T63) with quadrupled angular velocity $\Omega = 4\Omega^*$, the circulation statistics were sampled 5 times per day over 300 simulated days.

b. Determination of tropopause

The mean tropopause potential temperature $\overline{\theta}_t(y)$ was determined as the line in the interior atmosphere along which

$$\frac{|\Psi(y, \theta)|}{\max_\theta |\Psi(y, \theta)|} = 0.1. \tag{20}$$

The maximum absolute value $\max_\theta |\Psi(y, \theta)|$ of the streamfunction at each latitude occurs near the top of the surface layer and gives the magnitude of the vertically integrated mean equatorward mass flux $\overline{\rho}_\theta \overline{v}^*$ (cf. Fig. 2). Determining the tropopause potential temperature $\overline{\theta}_t(y)$ at each latitude as the potential temperature in the interior atmosphere at which the absolute value of the streamfunction $|\Psi(y, \theta)|$ amounts to 10% of the maximum value $\max_\theta |\Psi(y, \theta)|$ implies that 90% of the equatorward mass flux along surface-layer isentropes are returned as a poleward mass flux along interior

TABLE 2. Circulation statistics in simulations with idealized GCM. Extratropical mean values $\langle \cdot \rangle$ are mean values over latitudes poleward of $\hat{\phi}$ (see footnote 8). The last column gives the relative deviations of the potential temperature differences $-\langle (f/\beta)\partial_y \overline{\theta}_s \rangle$ expected according to the dynamical constraint (13) from the actual potential temperature differences $\langle \overline{\theta}_t - \overline{\theta}_s \rangle$. The asterisk denotes the reference parameter values listed in Table 1.

	$\hat{\phi}$	$\langle \overline{p}_t \rangle$ (hPa)	$\langle \overline{T}_t \rangle$ (K)	$\langle \overline{\theta}_t \rangle$ (K)	$\langle \overline{\theta}_s \rangle$ (K)	$\langle \overline{\theta}_t - \overline{\theta}_s \rangle$ (K)	$-\langle (f/\beta)\partial_y \overline{\theta}_s \rangle$ (K)	Error
Reference	29.4°	302.7	211.3	297.5	269.3	28.2	24.6	−0.13
γ = 0.6	26.6°	314.3	215.6	301.2	271.5	29.6	23.1	−0.22
0.7	26.6°	315.2	214.8	299.5	271.1	28.4	23.2	−0.18
0.8	26.6°	312.4	214.1	299.0	271.0	27.9	23.7	−0.15
0.9	26.6°	304.9	212.5	298.8	270.6	28.3	23.6	−0.16
1.1	29.4°	299.5	210.3	297.1	268.5	28.6	23.6	−0.17
1.2	29.4°	305.9	210.7	296.1	268.1	28.0	22.5	−0.20
1.3	29.4°	311.3	210.6	294.6	267.7	27.0	21.5	−0.20
1.4	29.2°	313.7	210.0	293.1	267.5	25.6	21.5	−0.16
Δ_h = 30 K	26.6°	314.1	211.7	295.2	277.6	17.6	15.0	−0.15
45 K	29.2°	309.5	210.6	294.8	272.8	22.0	18.1	−0.18
75 K	29.4°	296.1	211.5	299.6	265.3	34.3	30.8	−0.10
90 K	29.4°	290.2	212.1	302.2	261.2	41.0	37.2	−0.09
105 K	31.8°	281.7	211.9	304.0	256.4	47.6	44.1	−0.08
120 K	32.0°	281.2	212.5	305.3	251.6	53.7	50.6	−0.06
135 K	32.2°	275.4	212.9	307.8	247.2	60.6	57.0	−0.06
150 K	32.2°	272.3	213.9	310.1	242.2	67.9	65.6	−0.03
165 K	32.2°	267.3	214.2	312.4	239.6	72.8	72.8	0.00
180 K	34.6°	266.9	213.8	312.0	232.7	79.3	80.2	0.01
T_t^e = 160 K	32.2°	199.5	174.2	277.2	253.8	23.4	18.6	−0.20
170 K	32.0°	222.1	183.3	282.6	257.8	24.7	19.9	−0.19
180 K	32.0°	246.8	192.5	287.6	261.6	25.9	21.0	−0.19
190 K	29.4°	273.6	202.4	293.3	266.1	27.2	23.0	−0.16
210 K	29.2°	334.6	219.9	300.9	271.7	29.2	26.4	−0.09
220 K	26.4°	372.2	229.4	304.7	274.4	30.4	27.6	−0.09
230 K	23.8°	408.4	238.8	309.0	276.9	32.1	29.4	−0.08
240 K	23.8°	441.3	247.6	313.5	278.4	35.1	32.3	−0.08
τ_s = 4 days	29.4°	296.4	214.5	303.9	272.4	31.5	28.5	−0.10
15 days	29.2°	325.9	210.0	289.5	266.7	22.8	19.4	−0.15
30 days	26.6°	347.0	209.7	284.4	266.2	18.3	16.0	−0.12
40 days	26.6°	355.7	209.6	282.3	265.7	16.5	15.6	−0.06
50 days	26.4°	358.9	209.6	281.5	265.6	15.9	15.1	−0.05
k_d^0 = $2^{-6}\,k_d^{0*}$	29.4°	323.2	214.9	297.1	270.4	26.6	22.6	−0.15
$2^{-5}\,k_d^{0*}$	32.0°	330.4	214.8	295.1	269.5	25.6	20.7	−0.19
$2^{-4}\,k_d^{0*}$	32.0°	329.6	214.6	295.1	270.2	24.9	21.7	−0.13
$2^{-3}\,k_d^{0*}$	29.4°	321.0	212.5	294.3	269.4	24.9	20.5	−0.18
$2^{-2}\,k_d^{0*}$	29.4°	313.5	211.6	294.9	269.8	25.1	21.0	−0.17
$2^{-1}\,k_d^{0*}$	29.4°	307.8	211.4	296.2	269.5	26.7	22.2	−0.17
$2^1\,k_d^{0*}$	32.0°	296.3	211.6	299.3	269.1	30.3	28.9	−0.05
$2^2\,k_d^{0*}$	29.4°	289.2	212.2	302.6	269.9	32.7	31.0	−0.05
Ω = 0.5 Ω^*	40.6°	307.9	212.5	297.9	270.9	26.9	19.9	−0.26
$2^{-1/2}\,\Omega^*$	34.8°	304.5	211.6	297.3	269.7	27.6	24.3	−0.12
$2^{1/2}\,\Omega^*$	23.8°	311.8	212.3	296.7	270.5	26.2	23.5	−0.10
$2\,\Omega^*$	21.0°	312.5	213.7	298.5	274.9	23.6	22.5	−0.05
Ω = 4 Ω^* Δ_h = 120 K T_t^e = 225 K	14.0°	333.9	235.4	322.8	277.7	45.1	52.1	0.16

isentropes with potential temperature less than the tropopause potential temperature $\overline{\theta}_t(y)$. This criterion for determining the tropopause potential temperature is consistent with the mass flux constraint (3) from which the dynamical constraint (13) was derived; it is applicable to the extratropics and to the Tropics and subtropics.

Figure 5 shows the mass flux fraction on the left-hand side of the criterion (20) at typical tropical and extra-tropical latitudes in the reference simulation. As in the reference simulation, a well-defined extratropical tropopause forms in all simulations presented in Table 2. In all simulations, the extratropical tropopause determined by the mass flux criterion (20) marks a sharp transition between a troposphere and a stratosphere distinguishable by typical values of the isentropic mass flux divergence $\partial_y(\overline{\rho}_\theta \overline{v}^*)$ or of the isentropic density
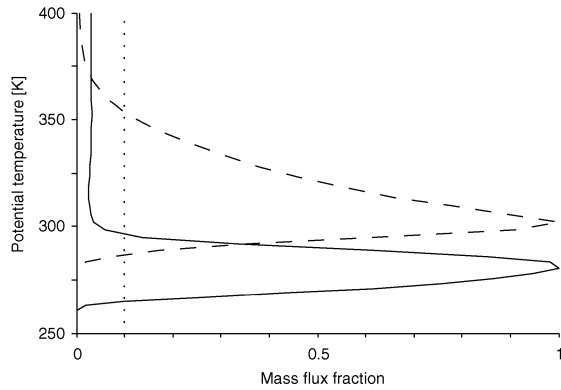
FIG. 5. Mass flux fraction $|\Psi(y, \theta)|/\max_\theta |\Psi(y, \theta)|$ in the reference simulation at latitudes 5° (dashed line) and 50° (solid line). The dotted line marks the critical mass flux fraction (0.1) used to determine the tropopause. The maxima of the mass flux fraction lie near the top of the surface layer.

$\overline{\rho}_\theta$. Because of the sharpness of this transition, the potential temperature $\overline{\theta}_t(y)$ of the extratropical tropopause determined by the mass flux criterion (20) is not very sensitive to the chosen value of the mass flux ratio. Only in the polar regions of some simulations is the transition between troposphere and stratosphere not very sharp (see footnote 8).

The tropical tropopause that forms in the simulations is less clearly defined than is the extratropical tropopause (cf. Fig. 5). The transition in typical values of the isentropic mass flux divergence $\partial_y(\overline{\rho}_\theta \overline{v}^*)$ or of the isentropic density $\overline{\rho}_\theta$ from the troposphere to the stratosphere is less sharp in the Tropics than in the extratropics, and the tropical tropopause potential temperature $\overline{\theta}_t(y)$ determined by the mass flux criterion (20) is more sensitive to the chosen value of the mass flux ratio. However, here we focus on the extratropical tropopause and thermal stratification.

c. Independence of extratropical and tropical thermal stratifications

Figure 6 shows the mean potential temperature and the tropopause in two simulations in which the re-

scaling factor γ of the pseudoadiabatic lapse rate was set to 0.6 and 1.4. Temperatures are relaxed toward the rescaled pseudoadiabatic temperature (19) in a narrow region around the equator. In the dynamical equilibria that develop in the simulations, the thermal stratification throughout the Tropics changes as the rescaling factor γ is varied. At a midtropospheric level ($\sigma \approx 0.5$) in the Tropics, the Brunt–Väisälä frequency changes from 1.5×10^{-2} s^{-1} for $\gamma = 0.6$ (Fig. 6a) over 1.1×10^{-2} s^{-1} for $\gamma = 1$ (Fig. 3b) to 0.6×10^{-2} s^{-1} for $\gamma = 1.4$ (Fig. 6b). The extratropical thermal stratification, however, is hardly affected by the changes of the tropical thermal stratification. For all values of the rescaling factor γ, the Brunt–Väisälä frequency at a midtropospheric level in midlatitudes is approximately 1.0×10^{-2} s^{-1}. Correspondingly, the tropical tropopause height changes significantly as the rescaling factor γ is varied, while the tropopause height in midlatitudes, sufficiently far away from the subtropics, changes only slightly (see Fig. 6 and Table 2).

The simulations for various values of the rescaling factor γ demonstrate that the extratropical tropopause height and thermal stratification do not depend on the tropical thermal stratification. The fact that, in the earth's atmosphere, the tropical and the extratropical Brunt–Väisälä frequencies are almost equal cannot be taken as evidence for a dynamical link between the extratropical and tropical thermal stratifications. The extratropical tropopause height and thermal stratification are set locally by extratropical processes, as was assumed in deriving the dynamical constraint (13).

d. Empirical eddy diffusivities

The derivation of the dynamical constraint (13) rests on the postulate that the eddy diffusivity D_i for potential vorticity exhibits no essential vertical structure within the troposphere and is, vertically averaged, approximately equal to the eddy diffusivity D_s for surface potential temperature. Figure 7 shows empirical eddy diffusivities in the simulation in which the near-surface thermal relaxation time τ_s was equal to the thermal relaxation time $\tau_i = 50$ days in the interior atmosphere. Plotted are the
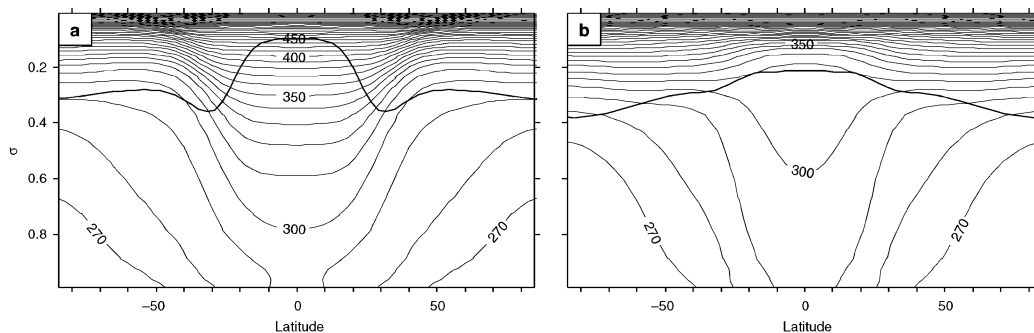

FIG. 6. Mean potential temperature (K) in simulations with a rescaled pseudoadiabatic lapse rate near equator and rescaling factors of (a) $\gamma = 0.6$ and (b) $\gamma = 1.4$. The thick lines mark the tropopauses.
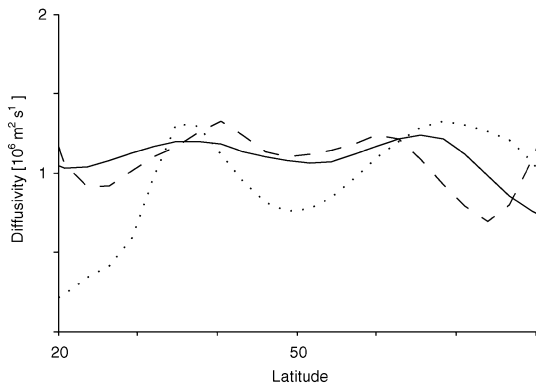
FIG. 7. Empirical eddy diffusivities in the simulation with near-surface relaxation time $\tau_s = 50$ days. Eddy diffusivity $\tilde{D}_s = -\overline{\overline{v_s' \theta_s'}}^s / \partial_y \overline{\theta}_s$ for surface potential temperature (solid line); eddy diffusivity $\tilde{D}_i = -\overline{\hat{v}\hat{P}}^* / \partial_y \overline{P}^*$ for potential vorticity in the surface layer (along the mean surface potential temperature, dashed line) and in the interior troposphere (along the $\overline{P}^* = 0.5$ PVU isoline of potential vorticity, dotted line).

empirical eddy diffusivity $\tilde{D}_s = -\overline{\overline{v_s' \theta_s'}}^s / \partial_y \overline{\theta}_s$ for surface potential temperature and the empirical eddy diffusivity $\tilde{D}_i = -\overline{\hat{v}\hat{P}}^* / \partial_y \overline{P}^*$ for potential vorticity in the surface layer (along the mean surface potential temperature) and in the interior troposphere (along a potential vorticity isoline that, in midlatitudes, lies roughly half way between the tropopause and the 95% isoline of the cumulative distribution of surface potential temperatures). The potential temperature at the lowest model level ($\sigma = 0.989$) is taken to represent the surface potential temperature. Figure 7 shows that, at least in a large-scale mean, these eddy diffusivities are indeed approximately equal. The empirical eddy diffusivity $\tilde{D}_i$ for potential vorticity does not exhibit pronounced vertical structure within the troposphere, except near the top of the surface layer, where the potential vorticity gradient $\partial_y \overline{P}^*$ changes sign and the diffusivity is ill-defined.

In the other simulations, the empirical eddy diffusivity for surface potential temperature and that for potential vorticity in the surface layer are generally approximately equal. The diffusivity for potential vorticity in the interior atmosphere in the subtropics and in lower extratropical latitudes tends to be smaller than the near-surface diffusivities when the near-surface thermal relaxation time τ_s is smaller than the interior relaxation time τ_i. [The near-surface diffusivities increase with decreasing thermal relaxation time near the surface, and the thermal relaxation time (18) near the surface approaches the interior relaxation time τ_i with increasing latitude.] In localized strongly baroclinic regions, the diffusivity for potential vorticity in the interior atmosphere often exceeds the near-surface diffusivities, usually in the vicinity of regions in which the potential vorticity gradient is so close to zero that it is difficult to estimate the diffusivities. As the baroclinicity is increased by increasing the equator-to-pole temperature difference Δ_h, the line along which the potential vor-

ticity gradient $\partial_y \overline{P}^*$ changes sign from negative values near the surface to positive values in the interior atmosphere moves upward, toward potential temperatures significantly above the 95% isoline of the cumulative distribution of surface potential temperatures. As a consequence, diffusivities become noisy and/or ill-defined in extended regions of the interior atmosphere. In these simulations, it is unclear to what extent the vertical structure of the diffusivity for potential vorticity is negligible. Overall, however, it appears that although the postulate regarding the eddy diffusivities is not quantitatively accurate latitude by latitude, it is a plausible starting point for understanding large-scale features of the turbulent mixing in the extratropical troposphere.

e. Validity of dynamical constraint

The circulation statistics listed in Table 2 indicate the degree to which the dynamical constraint (13) holds in the simulations with the idealized GCM. The quantities in Table 2 are extratropical mean values, denoted by angle brackets $\langle \cdot \rangle$.[8] Besides the potential temperatures of the tropopause $\langle \overline{\theta}_t \rangle$ and of the surface $\langle \overline{\theta}_s \rangle$ and the scaled surface potential temperature gradient $-\langle (f/\beta)\partial_y \overline{\theta}_s \rangle$ appearing in the dynamical constraint (13), Table 2 contains the pressure $\langle \overline{p}_t \rangle$ and the temperature $\langle \overline{T}_t \rangle$ of the extratropical tropopause. The table shows that, in the idealized GCM, the tropopause temperature $\langle \overline{T}_t \rangle$ is largely determined by the skin temperature T_t^e in radiative equilibrium. Given the skin temperature T_t^e, therefore, one can estimate how the tropopause pressure $\langle \overline{p}_t \rangle$ changes as the tropopause potential temperature $\langle \overline{\theta}_t \rangle$ changes, without the explicit radiative transfer calculation that would ordinarily be necessary to determine the tropopause pressure from a radiative constraint.

The deviations of the tropopause and surface potential temperatures from exact consistency with the dynamical constraint (13) are within the accuracy that can be expected given the approximations made in the derivation. The median absolute value of the relative deviation of the expected potential temperature difference $-\langle (f/\beta)\partial_y \overline{\theta}_s \rangle$ from the actual potential temperature difference $\langle \overline{\theta}_t - \overline{\theta}_s \rangle$ amounts to 13% and does

---

[8] The extratropical mean values $\langle \cdot \rangle$ in Table 2 are mean values over latitudes poleward of the latitude $\hat{\phi}$ at which the curvature $\partial_{\phi\phi} \overline{\theta}_t(\phi)$ of the temporal and zonal mean tropopause potential temperature $\overline{\theta}_t(\phi)$ is greatest. The latitude $\hat{\phi}$ of greatest curvature of the mean tropopause potential temperature $\overline{\theta}_t(\phi)$ is approximately the latitude of the core of the subtropical jet. As flow parameters are varied, the latitude $\hat{\phi}$ changes with the changing width of the Hadley cell (see Table 2). For the simulations with angular velocity $\Omega \geq 2\Omega^*$, with equator-to-pole temperature difference $\Delta_h = 30$ K, or with frictional wavenumber $k_a^0 \leq 2^{-4}k_a^{0*}$, the mean values $\langle \cdot \rangle$ are mean values over the extratropics poleward of $\hat{\phi}$ up to $|\phi| = 60°$; in these simulations, the tropopause is not clearly defined and/or the mean thermal stratification of the lower troposphere is statically unstable poleward of $|\phi| = 60°$. For all other simulations, the mean values $\langle \cdot \rangle$ are mean values over the extratropics poleward of $\hat{\phi}$ up to $|\phi| = 85°$.

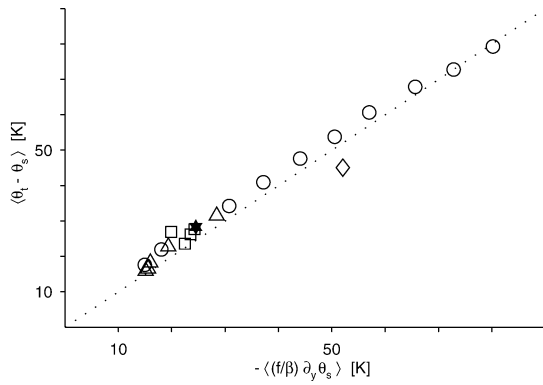FIG. 8. Extratropical mean values of the potential temperature difference $\langle \overline{\theta}_t - \overline{\theta}_s \rangle$ vs the expected potential temperature difference $-\langle (f/\beta)\partial_y \overline{\theta}_s \rangle$ in simulations with idealized GCM. Filled star, reference simulation; circles, variation of equator-to-pole surface temperature difference Δ_h; squares, variation of angular velocity Ω (with $0.5\Omega^* \leq \Omega \leq 2\Omega^*$); triangles, variation of near-surface relaxation time τ_s; and diamond, angular velocity $\Omega = 4\Omega^*$, equator-to-pole temperature difference $\Delta_h = 120$ K, and skin temperature $T_t^e = 225$ K.

FIG. 9. Extratropical mean values of the tropopause potential temperature $\langle \overline{\theta}_t \rangle$ vs the expected tropopause potential temperature $\langle \overline{\theta}_s - (f/\beta)\partial_y \overline{\theta}_s \rangle$ in simulations with idealized GCM. Filled star, reference simulation; open stars, variation of skin temperature T_t^e; triangles, variation of frictional wavenumber k_d^0; and crosses, variation of rescaling factor γ.

not exceed 26% in any simulation (Table 2, last column). Given the roughness of the approximations made in deriving the dynamical constraint (13), one might have expected the constraint to hold only as a scaling estimate, but it appears to hold as an approximate equality.

Figures 8 and 9 are scatterplots of quantities in Table 2 that, according to the dynamical constraint (13), should be pairwise equal. Figure 8 shows the potential temperature differences $\langle \overline{\theta}_t - \overline{\theta}_s \rangle$ plotted against the expected potential temperature differences $-\langle (f/\beta)\partial_y \overline{\theta}_s \rangle$ for the simulations in which the equator-to-pole surface temperature difference Δ_h, the angular velocity Ω, and the near-surface thermal relaxation time τ_s were varied. If the remaining simulations in Table 2 were included in Fig. 8, they would correspond to points scattered in the vicinity of the point that corresponds to the reference simulation (Fig. 8, filled star). To bring out more clearly the quantities that change in the simulations in which the rescaling factor γ of the pseudoadiabatic lapse rate, the skin temperature T_t^e, and the frictional wavenumber k_d^0 were varied, Fig. 9 shows the tropopause potential temperatures $\langle \overline{\theta}_t \rangle$ plotted against the expected tropopause potential temperatures $\langle \overline{\theta}_s - (f/\beta)\partial_y \overline{\theta}_s \rangle$. The approximate consistency of the tropopause and surface potential temperatures with the dynamical constraint (13) is evident from Figs. 8 and 9, as is a bias of the expected potential temperature difference $-\langle (f/\beta)\partial_y \overline{\theta}_s \rangle$ toward values less than the actual potential temperature difference $\langle \overline{\theta}_t - \overline{\theta}_s \rangle$. The following simulation results are notable:

1) A possible source of the bias of the dynamical constraint (13) is the approximation (12) for the isentropic density at the mean surface potential temperature. Surface inversions similar to the wintertime inversions that form in the earth's atmosphere at high latitudes form in most of the present simulations at
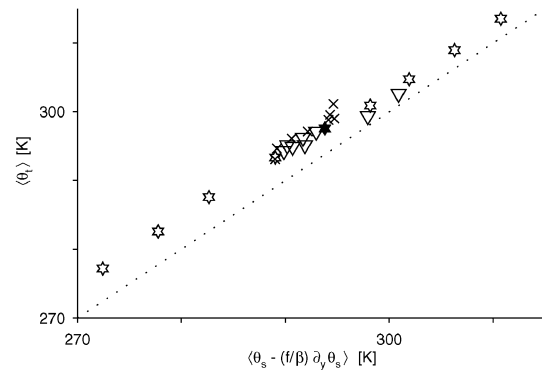
all latitudes, the inversions being most pronounced in the simulations with large equator-to-pole temperature difference Δ_h (cf. Held and Schneider 1999, section 4). Concomitant with surface inversions, there forms a statically very stable boundary layer with a sharp top that lies in all simulations below the 925-hPa pressure level. Within this boundary layer, the Brunt–Väisälä frequency is up to a factor of 2–3 greater than at the top of the boundary layer, resulting in low isentropic densities at the mean surface potential temperature and in the approximation (12) overestimating the actual isentropic density at the mean surface potential temperature by up to a factor of 6 in the extratropical mean (for $\Delta_h = 180$ K).

It appears that the limit in which the isentropic density and the thickness of the boundary layer approach zero is relevant for the simulations with strong surface inversions. In this limit, the top of the boundary layer plays the role of the surface in the arguments of section 2. The approximation (12) seems to provide a good approximation of the isentropic density at the potential temperatures that, in the mean, correspond to the top of the boundary layer, such that the dynamical constraint (13) is essentially unaffected by the error of the approximation (12) at the actual mean surface potential temperature. Consistent with this reasoning, the bias of the dynamical constraint (13) is reduced if the surface potential temperature gradient is replaced by the potential temperature gradient at the top of the boundary layer. For example, replacing the surface potential temperature gradient by the potential temperature gradient at the $\sigma = 0.925$ level reduces the median absolute value of the relative deviation of the expected potential temperature difference $-\langle (f/\beta)\partial_y \overline{\theta}_s \rangle$ from the actual potential temperature difference $\langle \overline{\theta}_t - \overline{\theta}_s \rangle$ from 13% to 5%, with increased absolute values of the relative deviations primarily

for those simulations in which no clear surface inversions form. The bias of the dynamical constraint (the mean of the relative deviations) reduces from -12% to -1%. However, given the roughness of the approximations made in the derivation of the dynamical constraint, this close agreement may not be completely explained by the arguments of section 2 and may be fortuitous.

2) According to the dynamical constraint (13), the potential temperature difference between tropopause and surface does not change as the angular velocity Ω of the planetary rotation is varied, provided the surface potential temperature gradient does not change. As the angular velocity Ω is varied in the simulations, at constant equator-to-pole surface temperature difference Δ_h in radiative equilibrium, the potential temperature difference $\langle \overline{\theta}_t - \overline{\theta}_s \rangle$ between tropopause and surface and the scaled surface potential temperature gradient $-\langle (f/\beta)\partial_y \overline{\theta}_s \rangle$ indeed do not change significantly (Fig. 8, squares). As in Thuburn and Craig's (1997) simulations with a comprehensive GCM, the tropopause height likewise does not change significantly as the angular velocity Ω is varied—despite significant changes in the atmospheric circulations. For example, the length scale of the energy-containing extratropical eddies decreases with increasing angular velocity Ω, and for $\Omega = 2\Omega^*$, each hemisphere contains two belts of surface westerlies that are clearly separated from each other by a belt of easterlies. In the simulation with angular velocity $\Omega = 4\Omega^*$, the tropopause height changes because the equator-to-pole surface temperature difference Δ_h and the skin temperature T_t^e in radiative equilibrium were also set to values different from the reference values. Nevertheless, the potential temperature difference $\langle \overline{\theta}_t - \overline{\theta}_s \rangle$ between tropopause and surface is within 16% of the expected value $-\langle (f/\beta)\partial_y \overline{\theta}_s \rangle$ (Fig. 8, diamond). In this simulation, the extratropics poleward of a narrow Hadley cell contain three alternating belts of surface westerlies and easterlies in each hemisphere and three associated upper-tropospheric jet cores, the jet cores, however, not being separated from each other by lines of zero wind.

3) With increasing skin temperature T_t^e in radiative equilibrium, the tropopause temperature in dynamical equilibrium increases, and the tropopause height decreases (Table 2). At the same time, the tropopause potential temperature $\langle \overline{\theta}_t \rangle$ increases in proportion to the increase of the expected tropopause potential temperature $\langle \overline{\theta}_s - (f/\beta)\partial_y \overline{\theta}_s \rangle$, although the bias of the expected tropopause potential temperature is evident (Fig. 9, stars).

4) With decreasing frictional wavenumber k_d^0, the zonal winds become increasingly barotropic, and the magnitudes of the extratropical eddy fluxes of potential vorticity along isentropes and of potential temperature along the surface decrease (cf. James and Gray

1986). Nevertheless, as the frictional wavenumber k_d^0 is varied by a factor of 256, the changes in tropopause height and tropopause potential temperature are relatively small and are consistent with the dynamical constraint (13) (Fig. 9, triangles), irrespective of the fact that the considerable changes of the barotropic shear of the zonal flow do affect the extratropical eddy fluxes.

5) Although the dynamical constraint derived from the baroclinic adjustment hypothesis that the quasigeostrophic potential vorticity gradient vanishes in the interior atmosphere is similar to the constraint (13), with the potential temperature gradient along pressure surfaces in the midtroposphere in place of the surface potential temperature gradient, the baroclinic adjustment constraint does not account for the simulated changes of the tropopause height and thermal stratification (cf. Thuburn and Craig 1997).[9] For example, as the equator-to-pole temperature difference $\underline{\Delta}_h$ is increased, the potential temperature difference $\langle \overline{\theta}_t - \overline{\theta}_s \rangle$ between tropopause and surface increases more strongly than linearly with the scaled potential temperature gradient $-\langle (f/\beta)\partial_y \overline{\theta}^p |_{p=p_m} \rangle$ along a midtropospheric pressure surface (e.g., for $p_m = 500$ or 600 hPa). Nonetheless, the similarity between dynamical constraints derived from baroclinic adjustment hypotheses and the dynamical constraint (13) may explain the relative success with which baroclinic adjustment constraints, despite their deficiencies (see, e.g., Barry et al. 2000), account for some aspects of the thermal stratification of the troposphere [see, e.g., Stone and Nemet (1996) or, for modifications due to moisture, Juckes (2000)].

The simulations span a wide range of atmospheric circulations, exhibiting, for example, multiple belts of surface westerlies in each hemisphere and surface temperature gradients 3 times as large as those on earth. In all these simulations, the dynamical constraint (13) appears to hold to within the degree of accuracy that could be expected, or perhaps with greater accuracy than could be expected, given the approximations made in the derivation.

f. Limits of validity of dynamical constraint

The dynamical constraint (13) is only valid if baroclinic eddies dominate the entropy transport in the extratropics and transport entropy efficiently enough to maintain a statically stable thermal stratification. If con-

---

[9] Among the technical differences between the study of Thuburn and Craig (1997) and the present study is the way in which the tropopause potential temperature and height are determined. Thuburn and Craig determine the tropopause according to the World Meteorological Organization's lapse rate criterion. If one determines the tropopause potential temperature in the present simulations according to the lapse rate criterion, the results summarized here only change in quantitative details, but not qualitatively.

vective or other dynamic fluxes dominate the entropy transport, the dynamical constraint (13) cannot be expected to be valid. For example, the dynamical constraint (13) is probably not valid for the Venus atmosphere, since the baroclinicity of the Venus atmosphere appears to be too weak for baroclinic eddies to be able to dominate the entropy transport.

Since the idealized GCM does not contain a representation of extratropical convective adjustment, the simulated extratropical thermal stratifications are statically unstable if the entropy transport due to baroclinic eddies does not suffice to maintain a statically stable thermal stratification. Extratropical thermal stratifications that are, in the mean, statically unstable develop, for example, if the equator-to-pole surface temperature difference Δ_h in radiative equilibrium is reduced to less than 30 K, or if the angular velocity Ω of the planetary rotation is reduced to less than 0.5 Ω^*. (The instantaneous thermal stratifications in simulations with greater baroclinicity are occasionally statically unstable, in particular near the surface, but in the mean, they are statically stable.) The fact that simulations with low baroclinicity are statically unstable in the mean limited the range of circulation regimes explored with the idealized GCM.

In addition to circulation regimes in which convective or other dynamic fluxes dominate the entropy transport, the dynamical constraint (13) also cannot be valid in circulation regimes in which the planetary vorticity gradient β does not affect baroclinic eddies. It is unclear how the tropopause height and thermal stratification would adjust if the energy-containing baroclinic eddies were so small compared with the planet radius that the planetary vorticity gradient β could effectively be set to zero.

5. Relevance of dynamical constraint for earth's atmosphere

The dynamical constraint (13) offers an explanation for the fact that in the earth's atmosphere, the equator-to-pole surface potential temperature difference is approximately equal to the potential temperature difference between tropopause and surface in midlatitudes (i.e., the lowest isentrope that crosses the tropopause near the poles grazes the surface in the subtropics or Tropics). However, to account quantitatively, for example, for seasonal variations of the extratropical tropopause, a dynamical constraint on the tropopause height and thermal stratification would need to take at least the thermodynamics of water vapor near the surface into account. For example, it may be possible to extend the theoretical developments of section 2 by considering mass fluxes along surfaces of constant moist entropy. It may also be necessary to take the entropy transport due to extratropical moist convection into account, as, for example, in the theory of Juckes (2000).

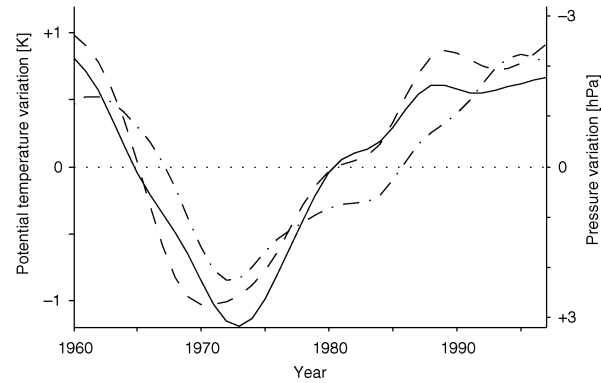Nevertheless, to the extent that interannual varia-

FIG. 10. Variations of annual mean tropopause potential temperature $\langle \overline{\theta}_t \rangle$ (solid line, left axis), expected tropopause potential temperature $\langle \overline{\theta}_s - (f/\beta)\partial_y \overline{\theta}_s \rangle$ (dashed line, left axis), and tropopause pressure $\langle \overline{p}_t \rangle$ (dashed–dotted line, right axis) about the mean values of the years 1960–97. Axis scales are chosen such that a potential temperature increment of 1 K corresponds to a pressure decrement of 2.7 hPa (cf. footnote 11).

tions of the water vapor content of the atmosphere can be neglected and that baroclinic eddies dominate the entropy transport in the extratropics, the dynamical constraint (13) should account for interannual variations of the extratropical tropopause. Figure 10 shows interannual variations of the tropopause potential temperature $\langle \overline{\theta}_t \rangle$ and of the expected tropopause potential temperature $\langle \overline{\theta}_s - (f/\beta)\partial_y \overline{\theta}_s \rangle$ in the extratropics of the Northern Hemisphere. The plotted variations are low-pass-filtered variations of annual mean values about the mean values of the years 1960–97.[10] The variations of the tropopause potential temperature $\langle \overline{\theta}_t \rangle$ follow the variations of the expected tropopause potential tem-

---

[10] Figure 10 is based on NCEP–NCAR reanalysis data (Kalnay et al. 1996) provided by the NOAA–CIRES Climate Diagnostics Center. The potential temperature at 850 hPa was taken as representing the surface potential temperature θ_s. The tropopause potential temperature θ_t and pressure p_t, determined according to the World Meteorological Organization's convention, were provided by the Climate Diagnostics Center. The extratropical mean values $\langle \cdot \rangle$ are annual mean values of the Northern Hemisphere, computed from monthly mean values over latitudes poleward of the latitude $\hat{\phi}$ at which the curvature $\partial_{\phi\phi} \overline{\theta}_t(\phi)$ of the monthly and zonal mean tropopause potential temperature $\overline{\theta}_t(\phi)$ is greatest. (The overbar $\overline{(\cdot)}$ here denotes a monthly and zonal mean, and angle brackets $\langle \cdot \rangle$ denote an annual and extratropical mean.) Latitudes up to 72.5°N are included in the extratropical mean values $\langle \cdot \rangle$. The variations about the mean values of the years 1960–97 were low-pass filtered by convolution of the time series with a Gaussian smoothing kernel of standard deviation 2.5 yr. Although the reanalysis includes upper-tropospheric observations from 1958 onward, data only from 1960 onward were used, since the scaled surface potential temperature gradient $-\langle (f/\beta)\partial_y \overline{\theta}_s \rangle$, a noisy time series, takes a value for 1959 that appears anomalously small. Because of the low-pass filtering, this anomalously small value, if included, would affect the analysis for later years. Results for the years before 1979, prior to the availability of satellite data, are to be interpreted cautiously because NCEP–NCAR reanalysis data for that period for the lower stratosphere are known to be biased (Santer et al. 1999). See Santer et al. (2003a,b) for further analyses of tropopause data and for comparisons with simulations.

perature $\langle \overline{\theta}_s - (f/\beta)\partial_y\overline{\theta}_s \rangle$, with an rms deviation of 0.2 K.

Variations of the surface potential temperature $\langle \overline{\theta}_s \rangle$ and of the scaled surface potential temperature gradient $-\langle (f/\beta)\partial_y\overline{\theta}_s \rangle$ both contribute to the variations of the expected tropopause potential temperature $\langle \overline{\theta}_s - (f/\beta)\partial_y\overline{\theta}_s \rangle$. The surface potential temperature $\langle \overline{\theta}_s \rangle$ decreased from 1960 to the early 1970s by about 0.3 K and increased from the early 1970s to the 1990s by about 1.0 K (cf. Jones 1994). The scaled surface potential temperature gradient $-\langle (f/\beta)\partial_y\overline{\theta}_s \rangle$ decreased from 1960 to the early 1970s by about 1.6 K and increased from the early 1970s to the 1990s by about 0.9 K, thus contributing to the variations of the expected tropopause potential temperature $\langle \overline{\theta}_s - (f/\beta)\partial_y\overline{\theta}_s \rangle$ with the same sign as the variations of the surface potential temperature $\langle \overline{\theta}_s \rangle$.

Included in Fig. 10 are the variations of the extratropical tropopause pressure $\langle \overline{p}_t \rangle$ about the mean value of the years 1960–97. Linearizing the relation $p = p_0(T/\theta)^{1/\kappa}$ between pressure, temperature, and potential temperature, one expects small changes $\delta\theta_t$ and δT_t of the tropopause potential temperature θ_t and of the tropopause temperature T_t to lead to changes of the tropopause pressure p_t of approximately

$$\delta p_t \approx \frac{p_t}{\kappa}\left(\frac{\delta T_t}{T_t} - \frac{\delta\theta_t}{\theta_t}\right).$$

For the years 1960–97, the rms deviation (0.18 K) of the low-pass-filtered annual mean tropopause temperature $\langle \overline{T}_t \rangle$ from the long-term mean (217.6 K) was a factor of 3.5 smaller than the rms deviation (0.62 K) of the low-pass-filtered annual mean tropopause potential temperature $\langle \overline{\theta}_t \rangle$ from its long-term mean (324.5 K). Therefore, variations of the tropopause pressure $\langle \overline{p}_t \rangle$ about the long-term mean (250.6 hPa) were dominated by variations of the tropopause potential temperature $\langle \overline{\theta}_t \rangle$, with $\delta\langle \overline{p}_t \rangle \approx -2.7$ hPa K$^{-1}\delta\langle \overline{\theta}_t \rangle$.[11] Figure 10 shows that variations of the tropopause pressure $\langle \overline{p}_t \rangle$ and of the tropopause potential temperature $\langle \overline{\theta}_t \rangle$ indeed follow this relation approximately, to within the error that is to be expected if one neglects the contribution of tropopause temperature variations $\delta\langle \overline{T}_t \rangle$ to pressure variations $\delta\langle \overline{p}_t \rangle$. Since variations of the surface potential temperature and of its gradient approximately determined variations of the tropopause potential temperature, which, in turn, approximately determined variations of the tropopause pressure, a large part of the interannual variations of the extratropical tropopause in the years 1960–97 appears to be dynamically linked to variations of the surface climate.

---

[11] The constant of proportionality between variations of the tropopause pressure $\langle \overline{p}_t \rangle$ and variations of the tropopause potential temperature $\langle \overline{\theta}_t \rangle$ is the derivative of the tropopause pressure with respect to potential temperature, $\partial_\theta p_t = -\kappa^{-1}(p_t/\theta_t)$, evaluated at the long-term mean: $-\kappa^{-1}$ (250.6 hPa/324.5 K) ≈ -2.7 hPa K^{-1}.

The dynamical constraint (13), then, accounts quantitatively for observed interannual variations of the extratropical tropopause and makes it possible to predict how the tropopause potential temperature and pressure change as the climate changes. However, convective entropy fluxes, which were neglected in the derivation of the dynamical constraint (13), may still play a role in the maintenance of the extratropical thermal stratification. With the reanalysis data, for example, Juckes's (2000) dynamical constraint cannot be distinguished from the dynamical constraint (13), provided an unspecified constant of proportionality in Juckes's dynamical constraint is adjusted to fit the data.

6. Implications for a turbulent energy cascade and for linear models of extratropical dynamics

The dynamical constraint (13) has implications for two characteristic length scales of geostrophic turbulence, the Rossby radius and the Rhines scale. Baroclinic energy generated by the differential heating of the atmosphere is converted into barotropic energy at the Rossby radius $L_R = NH_t/f$. From the Rossby radius, barotropic energy cascades upscale, up to a scale at which the inverse energy cascade is halted (see, e.g., Salmon 1998, chapter 6). Unless friction or the limited size of the planet halt the inverse energy cascade at a smaller scale, barotropic energy cascades up to the Rhines scale $L_\beta = (U'/\beta)^{1/2}$, with turbulent velocity scale U'. At the Rhines scale, energy is channeled into zonal jets and Rossby waves (Rhines 1975). Taking the anisotropy of the Rossby wave dispersion relation into account, one expects the Rhines scale L_β to approximate the meridional length scale of the energy-containing eddies (Vallis and Maltrud 1993).

To express the Rhines scale in terms of mean flow quantities, let us assume that the turbulent velocity scale U' is related to the velocity scale U of the mean flow in the upper troposphere by $U' \sim (L_\beta/L_R)^r U$, where the ratio L_β/L_R of Rhines scale to Rossby radius is a measure of the nonlinearity, or supercriticality, of the flow and r is a scaling exponent. Held and Larichev (1996) suggest $r = 1$ for the scaling exponent. Neglecting surface topography and using discrete approximations of the thermal wind relation and of the squared Brunt–Väisälä frequency,

$$U \approx -\frac{gH_t}{f\theta_0}\partial_y\overline{\theta}_s \quad \text{and} \quad N^2 \approx \frac{g}{\theta_0}\frac{\overline{\theta}_t - \overline{\theta}_s}{H_t}, \quad (21)$$

one finds the ratio of Rhines scale to Rossby radius:

$$\frac{L_\beta}{L_R} \sim \left|\frac{f}{\beta}\frac{\partial_y\overline{\theta}_s}{\overline{\theta}_t - \overline{\theta}_s}\right|^{1/(2-r)}. \quad (22)$$

For arbitrary values of the scaling exponent r, it follows that inasmuch as the dynamical constraint (13) on the tropopause height and thermal stratification holds, the

Rhines scale and the Rossby radius are of the same order of magnitude, $L_\beta/L_R \sim 1$.[12]

The coincidence of Rossby radius and Rhines scale implies that barotropic energy cannot go through a significant inverse cascade. The thermal stratification of the troposphere is such that the nonlinear eddy–eddy interactions that would give rise to an inverse energy cascade are inhibited. The reasoning that led to the dynamical constraint (13) did not presuppose nonlinear eddy–eddy interactions to be weak; hence, it offers an explanation for the historic successes of linear or weakly nonlinear models of large-scale extratropical dynamics and for the apparent absence of a significant inverse energy cascade in the troposphere (see, e.g., Boer and Shepherd 1983; Randel and Held 1991; Welch and Tung 1998).

For example, one could not have expected a priori that typical length scales and spatial structures of the most unstable baroclinic waves in linear models such as Eady's (1949) model or Charney's (1947) model resemble typical length scales and spatial structures of the energy-containing baroclinic eddies observed in the earth's atmosphere. In an atmosphere with strong nonlinear eddy–eddy interactions and with a significant inverse energy cascade, one would expect that typical length scales of the energy-containing eddies would be greater than those of the linearly most unstable waves, and there would be no necessary resemblance between the spatial structure of the energy-containing eddies and that of the linearly most unstable waves. The successes of linear and weakly nonlinear models in accounting for the structure of observed large-scale eddies in the extratropics may be a consequence of the atmospheric circulation organizing itself into a state in which nonlinear eddy–eddy interactions are weak.

7. Summary

A dynamical constraint on the extratropical tropopause height and thermal stratification has been derived by considerations of entropy fluxes, or isentropic mass fluxes. The condition that the circulation of mass along and across isentropes approximately closes within the

---

[12] In the simulations of section 4, the Rossby radius NH_t/f [with N estimated according to Eq. (21)], the Rhines scale $(U'/\beta)^{1/2}$ (with U' estimated from the vertically averaged eddy kinetic energy), and the mixing length $(\overline{\theta_s'^2})^{1/2}/|\partial_y\overline{\theta}_s|$ for surface potential temperature indeed covary and are of the same order of magnitude. How the three length scales vary with latitude depends on the method of averaging employed, but averaged over the extratropics, they differ by at most a factor of 2, despite variations of the mixing length by up to a factor of 6 across the simulations. In the simulations of Barry et al. (2002), the Rossby radius and Rhines scale likewise appear to be of the same order of magnitude, though in some of their simulations, the difference between Rossby radius and Rhines scale appears to be larger than in the present simulations. The reasons for the discrepancy between the simulation results are unclear; they may lie in different ways of averaging the quantities relevant for the computation of the Rossby radius and Rhines scale.

troposphere was taken as defining the tropopause. By means of a relation between isentropic mass fluxes and eddy fluxes, this condition on isentropic mass fluxes was transformed into a balance condition for eddy fluxes: upon vertical integration over the troposphere, the isentropic mass flux associated with the eddy flux of potential vorticity approximately balances the isentropic mass flux associated with the balanced eddy flux of surface potential temperature. A diffusive closure of the eddy fluxes combined with the postulate that the eddy diffusivity for potential vorticity exhibits no essential vertical structure within the troposphere and is, vertically averaged, approximately equal to the eddy diffusivity for surface potential temperature led to the dynamical constraint $\overline{\theta}_t - \overline{\theta}_s \approx -(f/\beta)\partial_y\overline{\theta}_s$.

A linear relation between the tropopause potential temperature and the surface potential temperature and its gradient, the dynamical constraint has a very simple form—a form that could not have resulted from similar considerations within quasigeostrophic theory. The mean potential vorticity balance of near-surface isentropes differs fundamentally from the mean potential vorticity balance of near-surface horizontal planes in quasigeostrophic theory. The postulated structure of eddy diffusivities that led to the present dynamical constraint is impossible in quasigeostrophic models.

A series of simulations with an idealized GCM showed that, across a wide range of atmospheric circulations, the dynamical constraint describes the relation between tropopause and surface potential temperatures well. The simulations pointed to the possibility of an earth-like extratropical climate in which baroclinic eddy fluxes maintain a statically stable thermal stratification and, in interaction with large-scale diabatic processes, lead to the formation of a sharp tropopause. In the simulations as in observational data, the empirical eddy diffusivity for potential vorticity varied only weakly across the extratropical tropopause, implying that the extratropical tropopause cannot be viewed as a kinematic mixing barrier. That a well-defined tropopause formed although the radiative equilibrium temperature in the simulations decreases smoothly and monotonically with height means that, as the simulations by Thuburn and Craig (1997) indicated, the radiative heating of the earth's stratosphere due to absorption of solar radiation by ozone is only of secondary significance for the existence of a tropopause, although it can modify the temperature and height of the tropopause. The simulations also showed that the extratropical tropopause height and thermal stratification are set locally by extratropical processes and do not depend on tropical processes. The postulate that the eddy diffusivity for potential vorticity exhibits no essential vertical structure within the troposphere and is, vertically averaged, approximately equal to the eddy diffusivity for surface potential temperature, although not quantitatively accurate latitude by latitude,

was seen to be a plausible starting point for understanding large-scale features of the turbulent mixing in the extratropical troposphere.

An analysis of observational data showed that the dynamical constraint, derived for an idealized dry atmosphere with stationary and axisymmetric circulation statistics, can also account for interannual variations of the tropopause height and thermal stratification in the extratropics of the earth's atmosphere. The agreement of the dynamical constraint with the observational data means that the dynamical constraint can be combined with a radiative constraint to compute the variations of the tropopause height and thermal stratification that are associated with interannual variations of the surface potential temperature.

The dynamical constraint implies that if baroclinic eddies determine the tropopause height and thermal stratification, an atmosphere organizes itself into a state in which nonlinear interactions among eddies are inhibited. Given that there is no reason a priori to suppose that nonlinear eddy–eddy interactions are weak, the inhibition of nonlinear eddy–eddy interactions offers an explanation for the historic successes of linear and weakly nonlinear models of large-scale extratropical dynamics—an explanation that rests on the postulate that the kinematic mixing properties of the baroclinic eddies exhibit no essential vertical structure. The fact that the dynamical constraint implies that the atmosphere organizes itself into a critical state with weak nonlinear eddy–eddy interactions intimates that there may exist a fundamental variational principle that would justify the postulate on eddy diffusivities and/or the dynamical constraint itself. What form such a variational principle might take remains to be investigated.

APPENDIX

Notation and Symbols

∂_ξ	Partial derivative with respect to coordinate ξ (unless otherwise noted, with horizontal derivatives understood as derivatives along isentropes if the argument depends on a vertical coordinate)
$\overline{(\cdot)}$	Temporal and zonal mean (along isentropes if the argument depends on a vertical coordinate)
$\overline{(\cdot)}^*$	Isentropic mean $\overline{(\rho_\theta \cdot)}/\overline{\rho}_\theta$ weighted by isentropic density ρ_θ
$(\hat{\cdot})$	Fluctuation $(\hat{\cdot}) = (\cdot) - \overline{(\cdot)}^*$ about density-weighted isentropic mean $\overline{(\cdot)}^*$
$\overline{(\cdot)}^s$	Temporal and zonal mean along surface
$(\cdot)'$	Fluctuation $(\cdot)' = (\cdot) - \overline{(\cdot)}^s$ about surface mean $\overline{(\cdot)}^s$
$\langle \cdot \rangle$	Extratropical mean
a	Planet radius
c_p	Specific heat at constant pressure
D_s, D_i	Eddy diffusivities for surface potential temperature and for potential vorticity on isentropes
f	Coriolis parameter $f = 2\Omega \sin(\phi)$
g	Gravitational acceleration
H_t	Tropopause height
$\mathcal{H}(\cdot)$	Heaviside step function
M	Montgomery streamfunction $M = c_p T + gz$
N	Brunt–Väisälä frequency
p, p_0	Pressure, constant reference pressure
P	Potential vorticity $P = (f + \zeta_\theta)/\rho_\theta$
Q	Material derivative of potential temperature $Q = D\theta/Dt$
R	Gas constant
t	Time
T	Temperature
u, v	Horizontal velocity components (eastward, northward)
U, U'	Mean velocity scale, turbulent velocity scale
$\mathbf{v}$	Horizontal velocity [$\mathbf{v} = (u, v, 0)$ in local Cartesian coordinates]
$\tilde{v}'_s$	Balanced meridional eddy velocity at the surface
x, y, z	Local Cartesian coordinates (eastward, northward, upward)
β	Meridional derivative $\beta = 2\Omega a^{-1} \cos(\phi)$ of Coriolis parameter
ζ_θ	Relative vorticity of horizontal flow along isentropes
θ, θ_0	Potential temperature $\theta = T(p_0/p)^\kappa$, constant reference potential temperature
θ_b	A potential temperature $\theta_b = \theta_b(y)$ less than the lowest potential temperature that occurs at a given latitude
θ_t	Tropopause potential temperature
κ	Adiabatic exponent $\kappa = R/c_p$

ρ Density

ρ_θ Isentropic density $\rho_\theta = -(g^{-1}\partial_\theta p)\mathcal{H}(\theta - \theta_s)$

$\overline{\rho}_\theta^0$ Mean isentropic density $\overline{\rho}_\theta^0 = \overline{\rho}_\theta(y, \overline{\theta}_s)$ at mean surface potential temperature $\overline{\theta}_s$

σ Terrain-following coordinate $\sigma = p/p_s$

ϕ Latitude

Ψ Streamfunction of mass flux $(\overline{\rho}_\theta \overline{v}^*, \overline{\rho}_\theta \overline{Q}^*)$

Ω Angular velocity of planetary rotation

REFERENCES

Andrews, A. E., and Coauthors, 2001: Mean ages of stratospheric air derived from in situ observations of CO_2, CH_4 and N_2O. *J. Geophys. Res.,* **106D,** 32 295–32 314.

Barry, L., G. C. Craig, and J. Thuburn, 2000: A GCM investigation into the nature of baroclinic adjustment. *J. Atmos. Sci.,* **57,** 1141–1155.

——, ——, and ——, 2002: Poleward heat transport by the atmospheric heat engine. *Nature,* **415,** 774–777.

Bartels, J., D. Peters, and G. Schmitz, 1998: Climatological Ertel's potential-vorticity flux and mean meridional circulation in the extratropical troposphere–lower stratosphere. *Ann. Geophys.,* **16,** 250–265.

Boer, G. J., and T. G. Shepherd, 1983: Large-scale two-dimensional turbulence in the atmosphere. *J. Atmos. Sci.,* **40,** 164–184.

Bourke, W., 1974: A multilevel spectral model. I. Formulation and hemispheric integrations. *Mon. Wea. Rev.,* **102,** 687–701.

Charney, J. G., 1947: The dynamics of long waves in a baroclinic westerly current. *J. Meteor.,* **4,** 135–163.

——, and M. E. Stern, 1962: On the stability of internal baroclinic jets in a rotating atmosphere. *J. Atmos. Sci.,* **19,** 159–172.

Corrsin, S., 1974: Limitations of gradient transport models in random walks and in turbulence. *Advances in Geophysics,* Vol. 18A, Academic Press, 25–60.

Durran, D. R., 1999: *Numerical Methods for Wave Equations in Geophysical Fluid Dynamics.* Texts in Applied Mathematics, Vol. 32, Springer, 465 pp.

Eady, E. T., 1949: Long waves and cyclone waves. *Tellus,* **1,** 33–52.

Emanuel, K. A., 1988: Observational evidence of slantwise convective adjustment. *Mon. Wea. Rev.,* **116,** 1805–1816.

——, 1994: *Atmospheric Convection.* Oxford University Press, 580 pp.

——, 2002: The role of water in atmospheric dynamics and climate. *Meteorology at the Millennium,* R. P. Pearce, Ed., International Geophysics Series, Vol. 83, Academic Press, 62–71.

Goody, R. M., and Y. L. Yung, 1989: *Atmospheric Radiation: Theoretical Basis.* 2d ed. Oxford University Press, 519 pp.

Hall, T. M., and R. A. Plumb, 1994: Age as a diagnostic of stratospheric transport. *J. Geophys. Res.,* **99D,** 1059–1070.

Haynes, P., and E. Shuckburgh, 2000: Effective diffusivity as a diagnostic of atmospheric transport. 2. Troposphere and lower stratosphere. *J. Geophys. Res.,* **105D,** 22 795–22 810.

——, J. Scinocca, and M. Greenslade, 2001: Formation and maintenance of the extratropical tropopause by baroclinic eddies. *Geophys. Res. Lett.,* **28,** 4179–4182.

Held, I. M., 1982: On the height of the tropopause and the static stability of the troposphere. *J. Atmos. Sci.,* **39,** 412–417.

——, 1999: The macroturbulence of the troposphere. *Tellus,* **51A–B,** 59–70.

——, and M. J. Suarez, 1994: A proposal for the intercomparison of the dynamical cores of atmospheric general circulation models. *Bull. Amer. Meteor. Soc.,* **75,** 1825–1830.

——, and V. D. Larichev, 1996: A scaling theory for horizontally homogeneous, baroclinically unstable flow on a beta-plane. *J. Atmos. Sci.,* **53,** 946–952.

——, and T. Schneider, 1999: The surface branch of the zonally averaged mass transport circulation in the troposphere. *J. Atmos. Sci.,* **56,** 1688–1697.

Holton, J. R., P. H. Haynes, M. E. McIntyre, A. R. Douglass, R. B. Rood, and L. Pfister, 1995: Stratosphere–troposphere exchange. *Rev. Geophys.,* **33,** 403–439.

Hoskins, B. J., M. E. McIntyre, and A. W. Robertson, 1985: On the use and significance of isentropic potential vorticity maps. *Quart. J. Roy. Meteor. Soc.,* **111,** 877–946.

James, I. N., and L. J. Gray, 1986: Concerning the effect of surface drag on the circulation of a baroclinic planetary atmosphere. *Quart. J. Roy. Meteor. Soc.,* **112,** 1231–1250.

Johnson, D. R., 1989: The forcing and maintenance of global monsoonal circulations: An isentropic analysis. *Advances in Geophysics,* Vol. 31, Academic Press, 43–304.

Jones, P. D., 1994: Hemispheric surface air temperature variations: A reanalysis and an update up to 1993. *J. Climate,* **7,** 1794–1802.

Juckes, M. N., 2000: The static stability of the midlatitude troposphere: The relevance of moisture. *J. Atmos. Sci.,* **57,** 3050–3057.

Kalnay, E., and Coauthors, 1996: The NCEP/NCAR 40-Year Reanalysis Project. *Bull. Amer. Meteor. Soc.,* **77,** 437–471.

Lindzen, R. S., 1993: Baroclinic neutrality and the tropopause. *J. Atmos. Sci.,* **50,** 1148–1151.

——, and B. Farrell, 1980: The role of the polar regions in global climate, and a new parameterization of global heat transport. *Mon. Wea. Rev.,* **108,** 2064–2079.

Lorenz, E. N., 1955: Available potential energy and the maintenance of the general circulation. *Tellus,* **7,** 157–167.

Mahlman, J. D., 1997: Dynamics of transport processes in the upper troposphere. *Science,* **276,** 1079–1083.

Nakamura, N., 1996: Two-dimensional mixing, edge formation, and permeability diagnosed in an area coordinate. *J. Atmos. Sci.,* **53,** 1524–1537.

Peixoto, J. P., and A. H. Oort, 1992: *Physics of Climate.* American Institute of Physics, 520 pp.

Phillips, N. A., 1954: Energy transformations and meridional circulations associated with simple baroclinic waves in a two-level, quasi-geostrophic model. *Tellus,* **6,** 273–286.

Randel, W. J., and I. M. Held, 1991: Phase speed spectra of transient eddy fluxes and critical layer absorption. *J. Atmos. Sci.,* **48,** 688–697.

Rhines, P. B., 1975: Waves and turbulence on a β-plane. *J. Fluid Mech.,* **69,** 417–443.

——, and W. R. Holland, 1979: A theoretical discussion of eddy-driven mean flows. *Dyn. Atmos. Oceans,* **3,** 289–325.

Salmon, R., 1998: *Lectures on Geophysical Fluid Dynamics.* Oxford University Press, 378 pp.

Santer, B. D., J. J. Hnilo, T. M. L. Wigley, J. S. Boyle, C. Doutriaux, M. Fiorino, D. E. Parker, and K. E. Taylor, 1999: Uncertainties in observationally based estimates of temperature change in the free atmosphere. *J. Geophys. Res.,* **104D,** 6405–6333.

——, and Coauthors, 2003a: Behavior of tropopause height and atmospheric temperature in models, reanalyses, and observations: Decadal changes. *J. Geophys. Res.,* **108,** 4002, doi: 10.1029/2002JD002258.

——, and Coauthors, 2003b: Contributions of anthropogenic and natural forcing to recent tropopause height changes. *Science,* **301,** 479–483.

Schneider, T., cited 2003: Zonal momentum balance, potential vorticity dynamics, and mass fluxes on near-surface isentropes. [Available online at www.gps.caltech.edu/~tapio/.]

Smith, K. S., and G. K. Vallis, 2002: The scales and equilibration of midocean eddies: Forced-dissipative flow. *J. Phys. Oceanogr.,* **32,** 1699–1720.

Stone, P. H., 1972: A simplified radiative-dynamical model for the static stability of rotating atmospheres. *J. Atmos. Sci.,* **29,** 405–418.

——, 1978: Baroclinic adjustment. *J. Atmos. Sci.,* **35,** 561–571.

——, and B. Nemet, 1996: Baroclinic adjustment: A comparison between theory, observations, and models. *J. Atmos. Sci.,* **53,** 1663–1674.

Thuburn, J., and G. C. Craig, 1997: GCM tests of theories for the height of the tropopause. *J. Atmos. Sci.,* **54,** 869–882.

——, and ——, 2000: Stratospheric influence on tropopause height: The radiative constraint. *J. Atmos. Sci.,* **57,** 17–28.

Treguier, A. M., I. M. Held, and V. D. Larichev, 1997: On the parameterization of quasigeostrophic eddies in primitive equation ocean models. *J. Phys. Oceanogr.,* **27,** 567–580.

Tung, K. K., 1986: Nongeostrophic theory of zonally averaged circulation. Part I: Formulation. *J. Atmos. Sci.,* **43,** 2600–2618.

Vallis, G. K., 1988: Numerical studies of eddy transport properties in eddy-resolving and parameterized models. *Quart. J. Roy. Meteor. Soc.,* **114,** 183–204.

——, and M. E. Maltrud, 1993: Generation of mean flows and jets on a beta plane and over topography. *J. Phys. Oceanogr.,* **23,** 1346–1362.

Weaver, C. P., and V. Ramanathan, 1995: Deductions from a simple climate model: Factors governing surface temperature and atmospheric thermal structure. *J. Geophys. Res.,* **100D,** 11 585–11 591.

Welch, W. T., and K. K. Tung, 1998: On the equilibrium spectrum of transient waves in the atmosphere. *J. Atmos. Sci.,* **55,** 2833–2851.

Xu, K.-M., and K. A. Emanuel, 1989: Is the tropical atmosphere conditionally unstable? *Mon. Wea. Rev.,* **117,** 1471–1479.

Yang, H., K. K. Tung, and E. Olaguer, 1990: Nongeostrophic theory of zonally averaged circulation. Part II: Eliassen–Palm flux divergence and isentropic mixing coefficient. *J. Atmos. Sci.,* **47,** 215–241.